Cell Reports
Medicine

Article

Single-cell RNA sequencing reveals distinct T cell populations in immune-related adverse events of checkpoint inhibitors

Graphical abstract

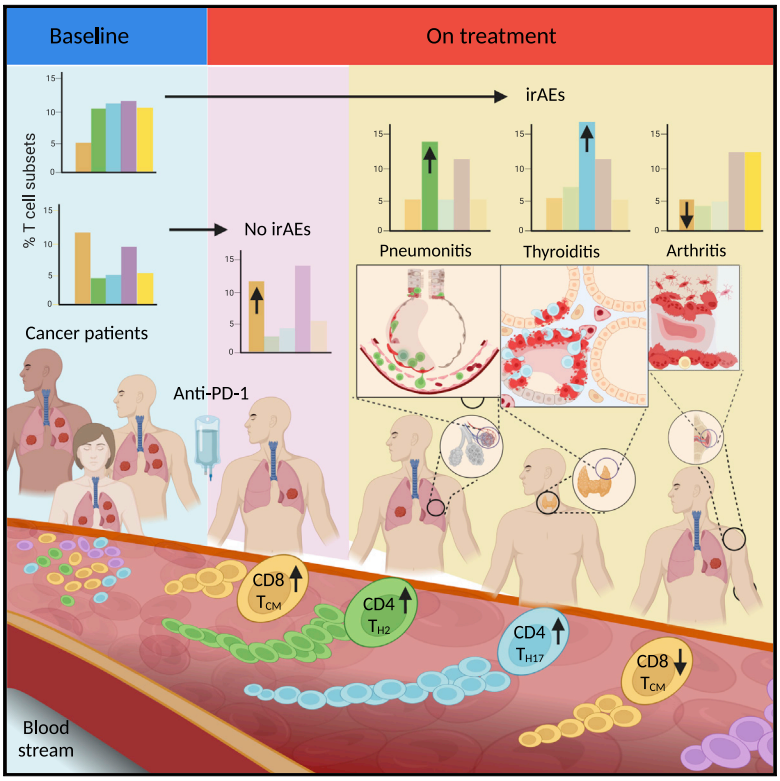

Highlights

- Selected T cell subsets are associated with organ-specific immune-related adverse events
- Patients with immune-related arthritis have lower levels of CD8 T_{CM} cells at baseline
- Patients with immune-related pneumonitis have more CD4 T_{H2} cells at baseline
- Patients with immune-related thyroiditis have more CD4 T_{H17} cells at baseline

Authors

Shoiab Bukhari, Brian S. Henick, Robert J. Winchester, ..., Matthen Mathew, Naiyer A. Rizvi, Adam Mor

Correspondence

am5121@columbia.edu

In brief

Bukhari et al. report that different subsets of T cells are associated with organ-specific immune-related adverse events of checkpoint inhibitors and that quantification and characterization of these populations of cells pre-treatment have the potential to serve as toxicity-specific predictive biomarkers.

Bukhari et al., 2023, Cell Reports Medicine *4*, 100868
January 17, 2023
https://doi.org/10.1016/j.xcrm.2022.100868

CellPress

Cell Reports Medicine

CellPress
OPEN ACCESS

Article

Single-cell RNA sequencing reveals distinct T cell populations in immune-related adverse events of checkpoint inhibitors

Shoiab Bukhari,[1] Brian S. Henick,[1,2] Robert J. Winchester,[1,3] Shalom Lerrer,[1] Kieran Adam,[1] Yevgeniya Gartshteyn,[3] Rohan Maniar,[2] Ziyan Lin,[4] Alireza Khodadadi-Jamayran,[4] Aristotelis Tsirigos,[4] Mary M. Salvatore,[5] Galina G. Lagos,[2] Steven L. Reiner,[6] Matthew C. Dallos,[2] Matthen Mathew,[2] Naiyer A. Rizvi,[2] and Adam Mor[1,2,3,7,*]

[1]Columbia Center for Translational Immunology, Columbia University Medical Center, New York, NY 10032, USA
[2]Herbert Irving Comprehensive Cancer Center, Columbia University Medical Center, New York, NY 10032, USA
[3]Division of Rheumatology, Department of Medicine, Columbia University Medical Center, New York, NY 10032, USA
[4]Applied Bioinformatics Laboratories and Genome Technology Center, Division of Advanced Research Technologies, NYU School of Medicine, New York, NY 10016, USA
[5]Department of Radiology, Columbia University Medical Center, New York, NY 10032, USA
[6]Departments of Microbiology & Immunology and Pediatrics, Columbia University Irving Medical Center, New York, NY 10032, USA
[7]Lead contact
*Correspondence: am5121@columbia.edu
https://doi.org/10.1016/j.xcrm.2022.100868

SUMMARY

PD-1 is an inhibitory receptor in T cells, and antibodies that block its interaction with ligands augment anti-tumor immune responses. The clinical potential of these agents is limited by the fact that half of all patients develop immune-related adverse events (irAEs). To generate insights into the cellular changes that occur during anti-PD-1 treatment, we performed single-cell RNA sequencing of circulating T cells collected from patients with cancer. Using the K-nearest-neighbor-based network graph-drawing layout, we show the involvement of distinctive genes and subpopulations of T cells. We identify that at baseline, patients with arthritis have fewer CD8 T_{CM} cells, patients with pneumonitis have more CD4 T_{H2} cells, and patients with thyroiditis have more CD4 T_{H17} cells when compared with patients who do not develop irAEs. These data support the hypothesis that different populations of T cells are associated with different irAEs and that characterization of these cells' pre-treatment has the potential to serve as a toxicity-specific predictive biomarker.

INTRODUCTION

PD-1 is an inhibitory receptor expressed on T cells and exploited by tumor cells to evade immune detection. By overexpressing PD-L1, a PD-1 ligand, tumor cells engage PD-1 on T cells, blocking its activation and function. This pathway has been effectively thwarted by monoclonal antibodies (Abs) targeting either PD-1 or PD-L1, with great success in unleashing an anti-tumor response.[1–4] Despite this powerful advance, there remain numerous challenges to immune checkpoint inhibitor (ICI) use that must be met to best advance the next generation of therapies. These challenges include increasing responsiveness to PD-1 and CTLA-4 blockade, uncovering additional targets to optimize pathway blockade, and, importantly, predicting and effectively managing immune-related adverse events (irAEs).[5–9] Patients who have a prior history of autoimmune disease are thought to be at increased risk for developing irAEs, but aside from this, no predictive factors have been identified to guide patients regarding their individual risk of toxicity with ICI treatment, a major unmet need in clinical decision-making. One of the ways to achieve these goals is better understanding and characterization of T cell responses during treatment with ICIs.

ICIs are associated with the development of irAEs that affect various tissues and organ systems throughout the body.[10] These acute and chronic inflammatory responses are thought to emerge because of the loss of the physiologic role played by immune checkpoints leading to unchecked T cell activation and loss of tolerance. irAEs are associated with significant morbidity and, in some cases, life-long disability. Some patients will require long-term immunosuppressive treatment, and others will have to withdraw from lifesaving anti-cancer therapy. Moreover, a particularly perplexing feature of irAEs is that they are often organ specific, with different organ systems being involved in different patients.[11,12] Although the molecular pathways that predispose to and trigger irAEs are incompletely delineated, it is well established that irAEs are mediated by T cell responses that drive tissue- and organ-specific inflammation and assist B cells in autoantibody production.[13,14] However, whether these T cell responses are similar in all irAEs, or whether distinctive responses are associated with different patterns of organ involvement, remains an unanswered question. Similarly, a related question is whether any features of the

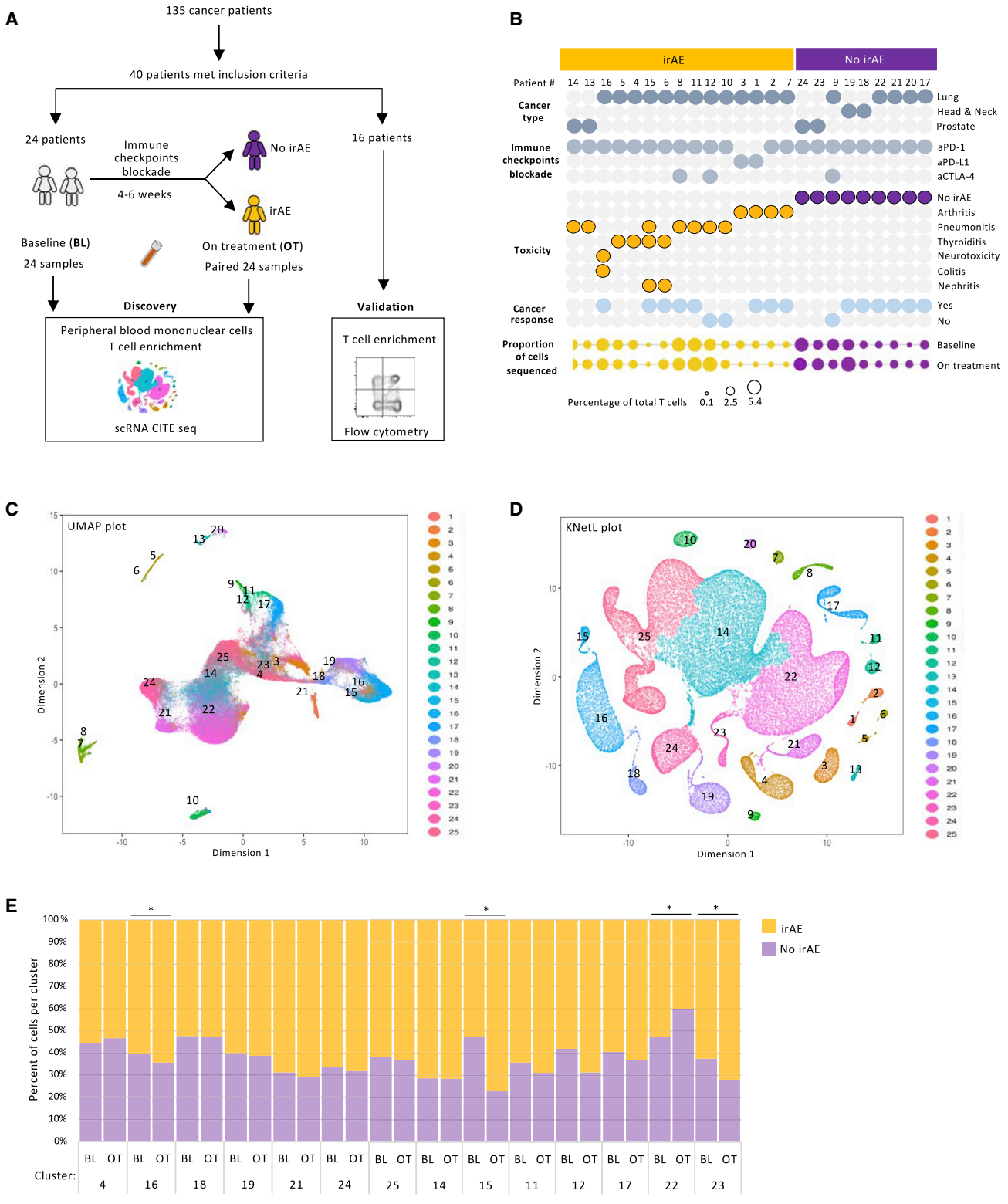

Figure 1. Dimensionality reduction approach to visualize single-cell RNA sequencing data of patients with immune-related adverse events

(A) Schematic workflow of study design.

(B) Clinical characterization of the patients.

(legend continued on next page)

pre-treatment immune system might allow one to predict the development of an irAEs.

To better understand the biology of T cell responses that develop during the course of ICI treatment and through the onset of irAEs, we applied a single-cell RNA sequencing (scRNA-seq) methodology to peripheral blood T cells prior to and during irAE development. We combined these analyses with a cellular indexing of transcriptomes and epitopes sequencing (CITE-seq) approach to stratify CD4 and CD8 T cells by naive and effector phenotypes in order to increase the specificity and sensitivity of our downstream analyses. Using this approach, we defined the molecular and cellular changes associated with T cell transition from self-tolerant to sensitized effector cells. These data should provide the basis for additional mechanistic studies of organ-specific irAEs.

RESULTS

Dimensionality reduction approach to visualize scRNA-seq data of patients with irAEs

We enrolled 40 patients with cancer into this study. These patients were divided into a discovery cohort, from which T cells were subjected to scRNA-seq, and a validation cohort, from which T cells were studied by flow cytometry (Figure 1A). The discovery group consisted of 24 patients from whom blood was collected before treatment with ICIs (at baseline) (Figure 1A). After 4–6 weeks of ICI treatment, 15 patients developed grade 2 or 3 irAEs, and from these patients, a second blood sample was collected (on treatment). Of the nine patients who did not develop AEs (no irAEs), the second matching blood sample was also collected after 4–6 weeks of the ICI treatment (total of 48 samples). The patients with no irAEs continued to have with no symptoms during the 12 month follow-up period. Out of the 24 patients, 18 had been diagnosed with lung adenocarcinoma, and 22 were treated with anti-PD-1 Abs (Figure 1B; Table S1A). Seven patients developed pneumonitis and were subsequently treated with high-dose corticosteroids, four patients presented with inflammatory polyarthritis, and four patients had thyroiditis, requiring hormonal replacement therapy. From each sample, a similar number of CD3 T cells were enriched using negative-selection sorting (Figures 1B and S1B). Initially, cells were subjected to CITE-seq with Abs tagged to CD4, CD8, CD27, and CD45RA (Figure S1A). Out of the 360,000 cells that were labeled, 135,287 CD3 T cells passed quality control (Figure S1C). Of these cells, 22,623 cells originated from patients with arthritis; 44,443 cells were collected from patients with pneumonitis; 12,913 cells came from patients with thyroiditis; and 51,177 cells were derived from patients with no irAEs.

Uniform manifold approximation and projection (UMAP) was used to display the data (Figure 1C). A K-nearest-neighbor-based network graph-drawing layout (KNetL) plot was generated to increase the resolution of the data and to better separate and characterize the 25 cellular clusters (Figure 1D). Overall, the distribution of the cells into clusters across individual patients was comparable, mitigating bias secondary to variation in the numbers of the sequenced cells (Figures S1B and S1D). While several populations of cells were enriched across all patients, other clusters were dominant among the patients that developed irAEs (Figures S1B and S1D). The relative distribution of some populations of cells through the different clusters was similar in samples collected at baseline and on treatment with ICIs (Figure 1E). However, few clusters showed statistically significant changes in their relative percentages between baseline and on treatment (Figure 1E). No major cluster distribution differences were observed between cells collected from male or from female patients (Figures S1F and S1G).

Gene-marker-based cluster annotation identifies effector, regulatory, and memory subsets of peripheral T cells

Twenty-five clusters were annotated using the iCellR pipeline (Figure S1E).[15] Fourteen clusters expressed the gene CD3E, of which six were dominated by CD8A and eight revealed high levels of the CD4 transcript (Figures 2A, 2D, and S1E). Based on reported gene markers (Table S2), within the CD8 T cells, naive cells (cluster 21) were characterized by the expression of CD45RA, CCR7, SELL (CD62L), and LEF1 (Figures 2A and S2A). The cells with the features of central memory CD8 T cells (cluster 4), beside containing CCR7, SELL, and CD27, expressed CD44, CXCR3, FAS, and high levels of CD28 transcripts. A subset of effector CD8 T cells (cluster 16) expressed TBX21 and cytotoxic markers such as GZMB, KLRD1, and PRF1 mRNA, along with the highest expression of CD3E. Complementary to the central memory CD8 T cells, the cells with the features of effector memory CD8 T cells (cluster 19) displayed EMOS, GZMK, and IFNG, highlighting their dampened, yet potential, cytotoxic activity. Interestingly, mucosal-associated invariant T cells (cluster 18) were discovered in the blood of all patients (Figure S2A). A cluster of cells expressing GATA3 suggested a commitment to CD8 T helper cells (cluster 24).

Among the CD4 T cell lineages, 8 clusters were annotated based on published markers (Table S2; Figure 2B). Three meta clusters comprised of cells expressing genes associated with T_{H1} and T_{H2} cells (cluster 25), T_{H17} cells (cluster 14), and naive cells (cluster 22) occupied most of the CD4 projections. The hybrid population of T_{H1} and T_{H2} cells was characterized by the expression of AREG, GATA3, PTGDR2, and CXCR3, known features of helper CD4 T cells (Figures 2A and S2A).[16–19] Cluster 14 expressed genes that were mainly involved in T_{H17} responses (further details in Figure 4). As expected, the majority of the peripheral CD4 T cells resembled naive cells (cluster 22), characterized also by the expression of the transcription factors TCF7 and LEF1 and the chemokine receptor CCR7. Surprisingly, a cytotoxic CD4 cluster expressing GZMB, GZMH, PRF1, and TBX21 was noted (cluster 15). While the classic regulatory T cells (clusters 17 and 11) showed high levels of FOXP3, IL2RA, and CTLA4,

(C and D) UMAP (C) and KNetL projection (D) of 135,287 T cells from patients with and without irAEs.

(E) Percentage variation in T cells between the baseline and on treatment within the cohorts of patients with no irAEs and with irAEs (paired t test).

Statistical significance for paired comparisons was performed by Student's t test applying Wilcoxon matched-pairs signed rank test, p value reported, one-tailed. Data are presented as mean ± SD. p value, exact, two-tailed. *$p < 0.05$, **$p < 0.01$, ***$p < 0.001$.

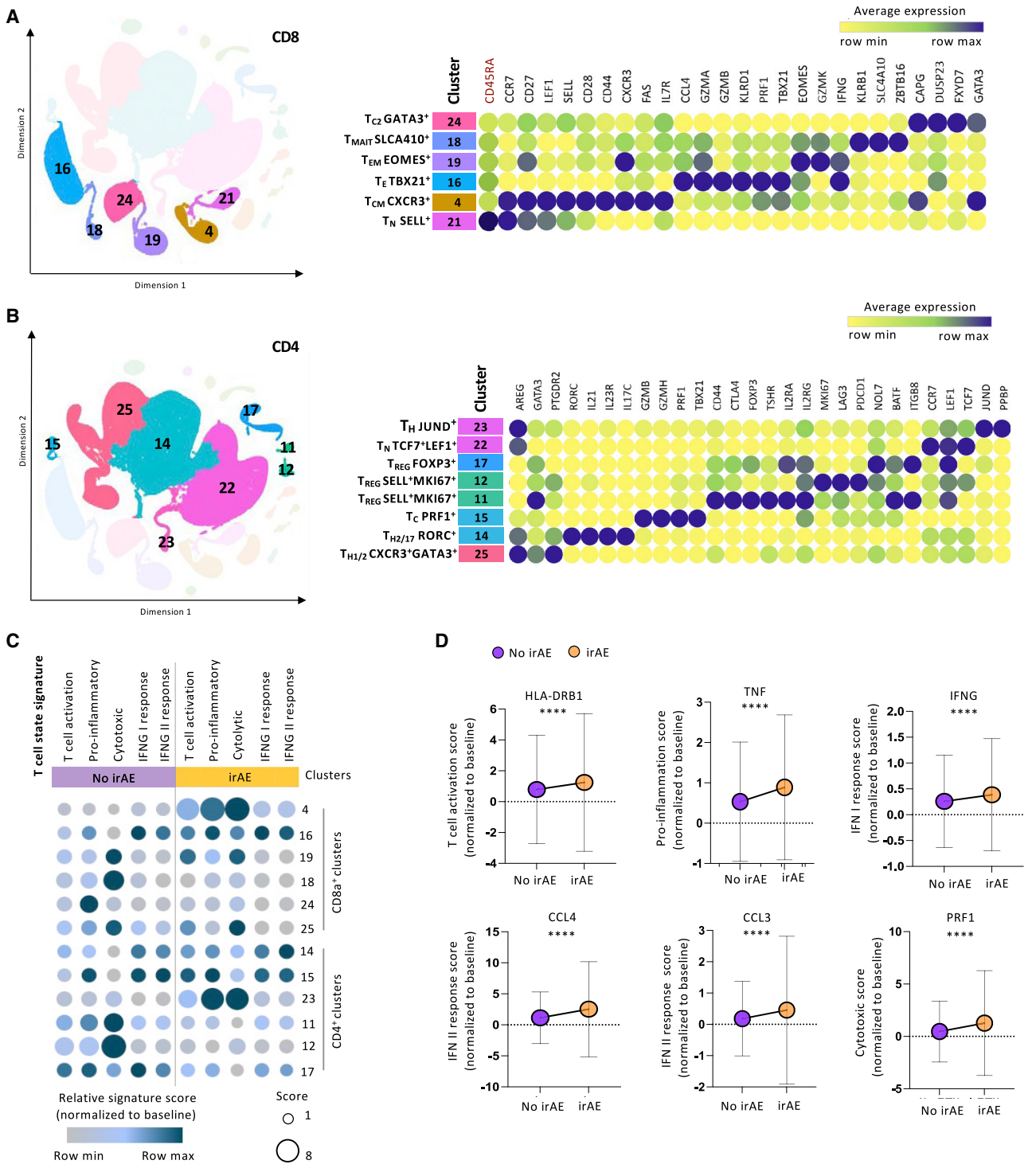

Figure 2. Gene-marker-based cluster annotation identifies effector, regulatory, and memory subsets of peripheral T cells

(A and B) KNetL plot schematic of clusters according to the expression levels of CD8A with a corresponding heatmap showing the expression of selected markers in CD8A clusters (CD45RA in red fonts indicates the CITE-seq-based protein expression) (A) and CD4 clusters (B).

(C) Heatmap-dot plot indicating the association between T cell states and clusters based on the relative signature score variabilities.

(D) Dot plot showing the comparison of T cell states between the cohorts of patients with no irAEs and with irAEs based on the marker gene scores (unpaired t test).

For unpaired comparisons, statistical significance was performed by Student's t test applying Mann-Whitney test. Data are presented as mean ± SD. p value, exact, two-tailed, the center lines denote the mean of SD. ****$p < 0.0001$.

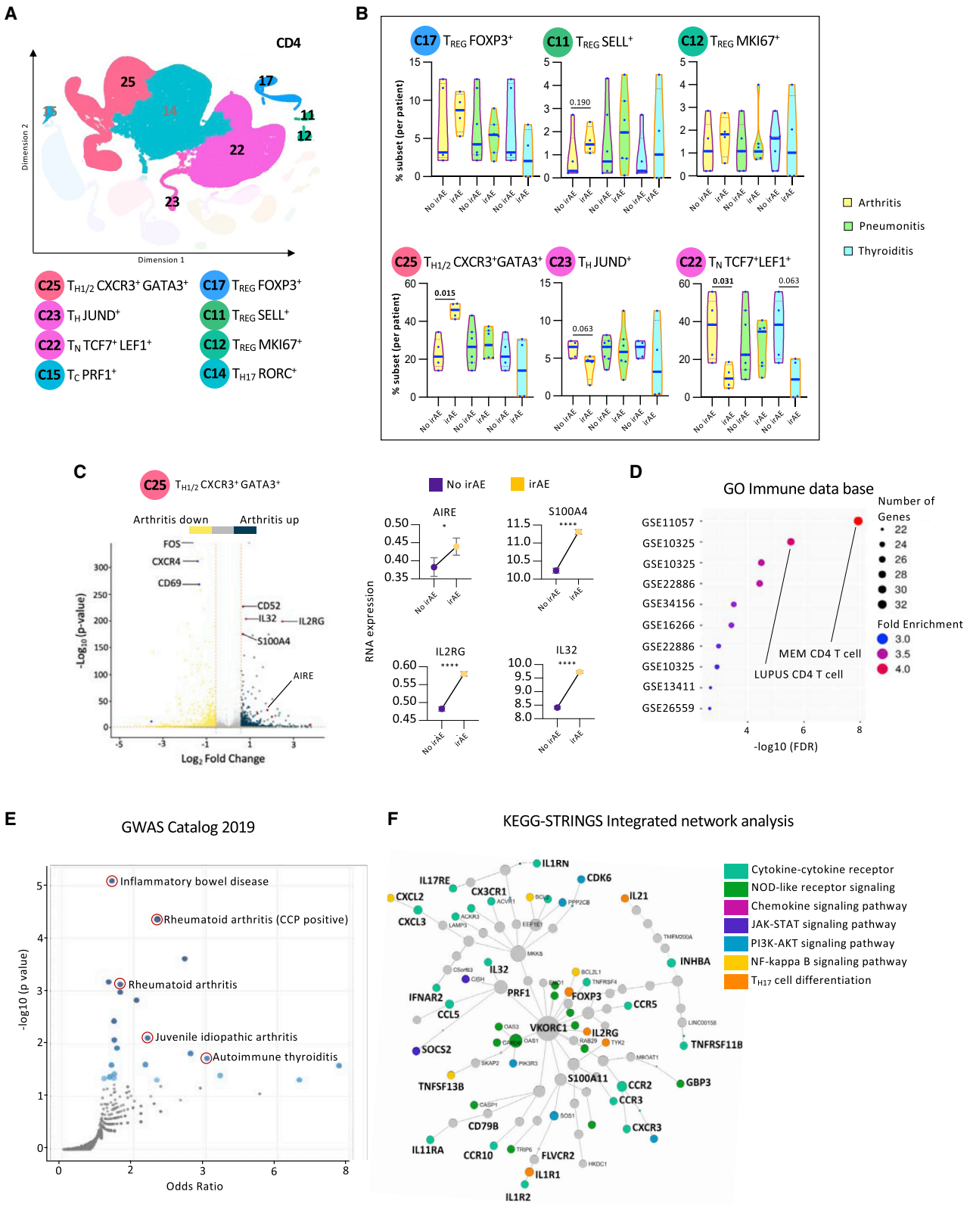

(legend on next page)

cluster 12 was described as regulatory-like cells based on the expression of shared regulatory genes (Figure S2B) while having relatively lower levels of FOXP3 and IL2RA expression.[20] Minor subsets of cells such as gamma delta and double-positive T cells were detected as well (Figure S3D). To confirm the rigor of our cluster annotations, we performed nearest-neighbor analysis for each cluster (Figure S2C). Through this analysis, we calculated the distance between the clusters obtained by each gene set used for cluster annotation and ranked the subsets based on that score (Figure S2C).

To further investigate the variability in the T cells between the patients with and without irAEs, we performed gene set signature analysis. Functional annotation (based on the T cell states and gene signatures) revealed association of irAEs' T cells with genes associated with T cell activation and cytokine secretion compared with no irAEs' T cells (Figure 2C). Cluster 4 (central memory T [T_{CM}] CXCR3$^+$), 16 (effector T [T_E] TBX21$^+$), 15 (cytotoxic T [T_C] PRF1$^+$), and 23 (helper T [T_H] JUND$^+$) had more cytotoxic and proinflammatory genes in the patients with irAEs compared with patients with no irAEs, while clusters 11 (regulatory T [T_{REG}] SELL$^+$MKI67$^+$), 12 (T_{REG} SELL$^+$MKI67$^+$), and 18 (mucosal-associated invariant T [T_{MAIT}] SLCA410$^+$) showed higher expression of activation genes in the patients with no irAEs compared with the irAE group. Further, we show that genes associated with T cell states (such as HLA-DRB1, TNF, IFNG, CCL4, CCL3, and PRF1) were highly expressed in the patients with irAEs even after normalization to baseline expression levels (Figure 2D). Altogether, these findings suggest that the population of T cells in the irAE groups were more likely to be associated with effector functions, while the cells of the no irAE groups were more likely to be associated with regulatory functions secondary to PD-1 blockade.

Patients with immune-related arthritis have higher percentages of CD4 T_H cells at baseline

Among the eight CD4 clusters previously annotated (Figure 3A), no major differences in the total percentages of CD4 T cells were noted (Figure S3Ai). The patients in the irAE-negative groups were selected to match the cancer types to patients in the arthritis, pneumonitis, and thyroiditis groups (Figure S3Aii). Although patients with thyroiditis had higher levels of CD4 T cells compared with patients with pneumonitis and arthritis, these differences were not significant (Figure S3Aii). Interestingly, patients with multiple organs afflicted by irAEs had lower levels of CD4 T cells than patients with no clinical toxicities (Figure S3Aiii), and by multiple comparison analysis, we show that this was statistically significant in one of the comparative components (Figure S3Aiv).

Analyzing the distribution of T cells in the different CD4 clusters revealed no differences at baseline between patients with irAEs and no irAEs (Figure S3B). However, stratifying the data by organ-specific irAEs, it became clear that patients with arthritis had significantly more $T_{H1/2}$ CXCR3$^+$GATA3$^+$ cells (cluster 25), more T_{REG} SELL$^+$ cells (cluster 11), fewer T_H JUND$^+$ cells (cluster 23), and fewer naive T (T_N) TCF7$^+$LEF1$^+$ cells (cluster 22) at baseline than patients from the corresponding irAE-negative group (Figure 3B). Differences in the percentages of these clusters did not hold for patients with pneumonitis and thyroiditis. These differences in subset percentages were not due to the gender or type of ICIs used (Figure S3C). These data suggest that enhanced T cell subset transition from naive to effector cells, specifically in patients who developed arthritis, can serve as evidence of pervasive immune responsiveness, as reflected by the predominance of later developmental stages.

The most significant baseline cluster that differentiated patients with arthritis from patients that did not develop irAEs was 25, $T_{H1/2}$ CXCR3$^+$GATA3$^+$. Further analysis of the genes that defined this specific cluster revealed significant upregulation of inflammatory genes such as IL32, IL2RG, and AIRE (Figure 3C). Performing ontology analysis on upregulated genes in $T_{H1/2}$ CXCR3$^+$ GATA3$^+$ of patients with arthritis revealed a significant overlap with genes related to autoimmune and other activated CD4 T cell conditions (Figure 3D). Moreover, through browsing a genome-wide association study (GWAS) catalog, we discovered that the same upregulated genes that characterized cluster 25 were overrepresented also in T cells from patients with other autoimmune diseases (Figure 3E), suggesting a potential mechanistic role in the pathogenesis of irAEs. Finally, through KEGG-Strings network analysis, we discovered that most the genes that defined cluster 25 were associated with specific signaling pathways that were previously shown to be involved in inflammatory arthritis (Figure 3F).

Selected subsets of CD4 T_H cells are associated with organ-specific irAEs

The analysis of cluster 14 (Figure S4A) revealed that in patients with thyroiditis, a higher percentage of CD4 T_H cells expressed high levels of RORC and interleukin-21 (IL-21) (Figure 4A). This expression pattern suggested that cluster 14 was a meta-cluster that contained cells with interesting features other than RORC expression (Figure S4B). To gain a better insight into this population, we subclustered the cells of cluster 14 into 6 additional subclusters (Figure 4B). Subclusters sC3, sC4, sC5, and sC6

Figure 3. Patients with immune-related arthritis have higher $T_{H1/2}$ cells and lower percentages of naive CD4 T cells at baseline

(A) Representative KNetL plot of annotated CD4 T cell clusters.

(B) Mean percentage of cells in six CD4 T cell subsets across the different clinical outcomes: arthritis, pneumonitis, and thyroiditis at baseline (unpaired t test).

(C) Volcano plot highlighting the up-regulated and down-regulated genes in cluster 25 of patients with arthritis, with paired-dot plots comparing the RNA expression of upregulated genes between no-irAE and arthritis groups.

(D and E) Gene Ontology (GO) analysis for differential genes present in cluster 25 from patients with arthritis for enriched terms from Immune.MSigDB (D) and from the GWAS Catalog 2019 (E).

(F) Pathway analysis of differentially expressed genes in cluster 25 from patients with arthritis using integrative KEGG-String platform.

Statistical significance for unpaired comparisons was performed by Student's t test applying Mann-Whitney test. Data are presented as mean ± SEM. p value, exact, two-tailed, the center lines denote the mean of SEM. *$p < 0.05$, ****$p < 0.0001$.

CellPress
OPEN ACCESS

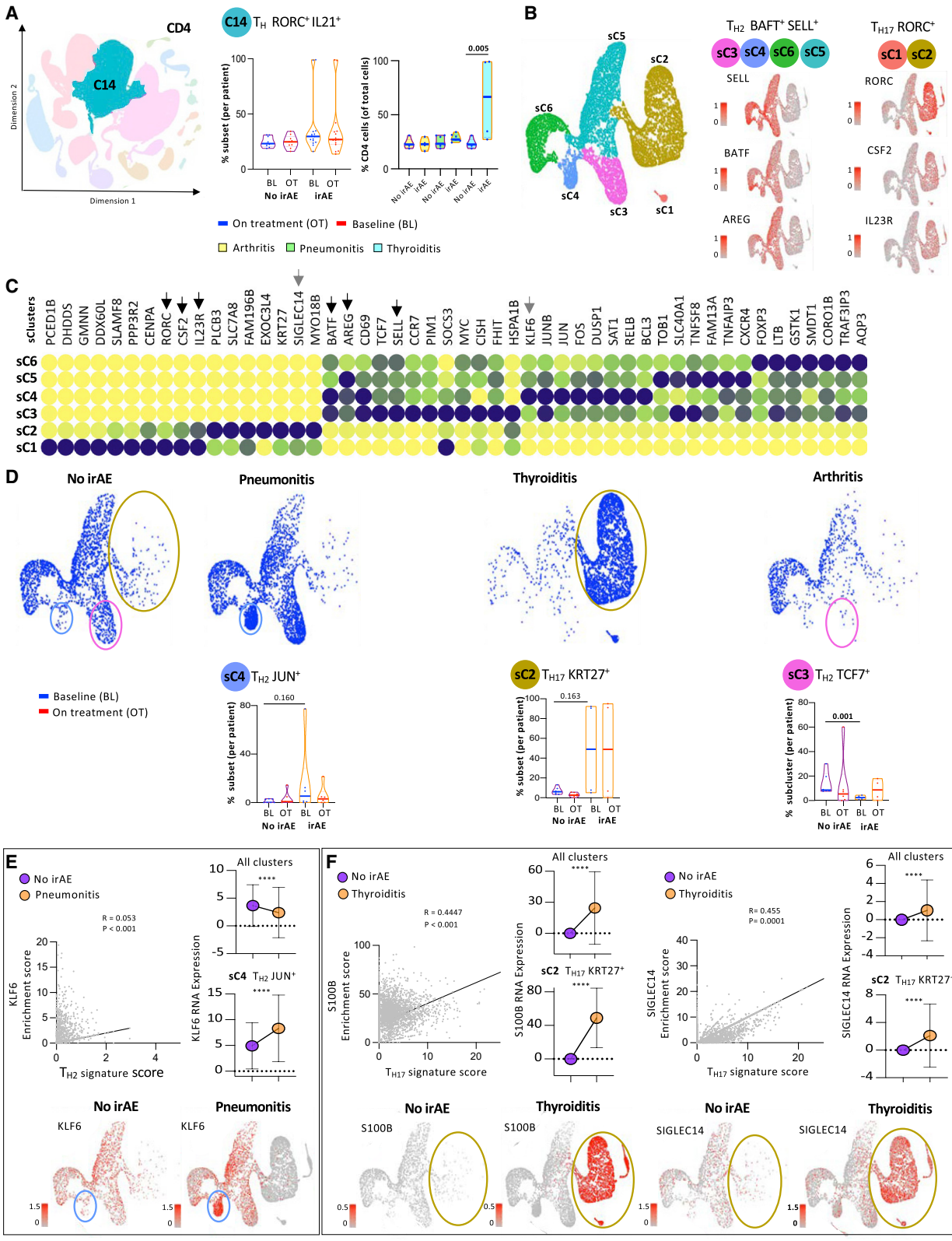

(legend on next page)

expressed genes that were strongly associated with T_{H2} cells (Figures 4B and 4C). Likewise, subclusters sC1 and sC2 conveyed genes correlated with T_{H17} cells and genes associated with pathogenic features highlighted by the expression of IL-23R and CSF2 (Figures 4B and 4C).[21,22] Most striking was the fact that while patients with arthritis had low sC3 cells (T_{H2} $TCF7^+$) at baseline, patients with pneumonitis collectively had more sC4 T cells (T_{H2} $CCR7^+$), and patients with thyroiditis had more sC1 T (T_{H17} $SLAMF8^+$) and sC2 T cells (T_{H17} $KRT27^+$), suggesting that different cellular subclusters are associated with distinct organ-specific irAEs (Figure 4D, S4A, and S4B). In terms of marker gene association, KLF6, a gene distinctive to the T_{H2} JUN^+ cells, correlated to some degree with the canonical T_{H2} signature score (CD4, GATA3, CXCR4, and AREG). The correlation coefficient was not strong, but nevertheless, higher mRNA expression KLF6 was noted in patients with pneumonitis (Figure 4E). Similarly, S100B and SIGLEC14, marker genes characteristic of T_{H17} $KRT27^+$ cells in the thyroiditis group, correlated with the T_{H17} signature score (CD4, RORC, and IL-23R) (Figure 4F). The ability to genetically differentiate between the types of irAEs is demonstrated through a heatmap and a Venn diagram showing 1,011, 1,162, and 628 genes distinctive to thyroiditis, pneumonitis, and arthritis, respectively (Figure S5A) This finding is also validated through principal-component analysis (PCA). Further, the set of differentially expressed genes between the three clinical groups was found to collectively enrich for CD4 subsets associated with activation phenotype (Figure S5B).

Patients with inflammatory arthritis have lower levels of CD8 T_{CM} cells at baseline

Six CD8 T cell clusters were annotated using the KNetL plot (Figure 5A). There were no differences in the proportion of total CD8 T cells between the baseline and the on-treatment groups (Figure S6Ai). The patients in the irAE-negative group were selected to match cancer types with the arthritis, pneumonitis, and thyroiditis groups (Figure S6Aii). Patients with pneumonitis and thyroiditis had lower, but not significant, levels of CD8 T cells at baseline and on treatment compared with patients with arthritis (Figure S6Aii). When analyzing patients with multi-organ irAEs, the levels of CD8 T cells were higher both at baseline and on treatment with ICIs compared with patients with single-organ irAEs (Figures S6Aiii and S6Aiv).

To better identify CD8 T cell clusters that could differentiate between patients with or without irAEs, we analyzed the distribution of cells within each cluster compared with the recruitment parameters. Patients with irAEs had less CXCR3-expressing central memory-like T cells (cluster 4) at baseline and on treatment (Figure S6B). No major differences in the cluster distribution were observed with the other population of cells. However, patients with arthritis had extremely low levels of T_{CM} cells (cluster 4) at baseline, suggesting that the evaluation of this cluster could serve as a clinical predictive biomarker (Figure 5B). Interestingly, the same patients had more effector (cluster 16) and effector memory (cluster 19) T cells at baseline. The patients with pneumonitis had fewer cells with features of effector memory T cells (cluster 19) than the patients who did not develop toxicity. The patients who developed thyroiditis had non-significant lower levels of effector cells (cluster 16) at baseline (Figure 5B). No other differences in the distribution of the CD8 T cell clusters were observed in the on-treatment group (Figure S6B). There were no differences in cluster C16 and cluster C4 based on the type of drug given or the gender of the patients (Figure S6C).

To better understand cluster 4, we show by volcano plot that most of the differentially expressed genes derived from patients did not developed arthritis (Figure 5C). These genes were subjected to Gene Ontology analysis and, interestingly, were associated with regulatory functions (Figure 5D). The contribution of this cluster to overall T cell suppression phenotype is further demonstrated through comparison of T cell suppressor signature scores between patients with arthritis and no irAEs (Figure 5E). Like other central memory populations, the genes in this cluster were associated with IL-3 and IL-5 secretion[24] and class I signaling[25] (Figure 5F).

To validate the observation that patients with arthritis had low CD8 T_{CM} cells at baseline at the protein level, we analyzed by flow cytometry T cells collected for a second cohort of 16 patients treated with PD-1 blockade (Figures 1A and 5G). Consistent with the analysis based on gene transcription, patients who developed arthritis had less naive and CD8 T_{CM} cells and more effector memory and terminally differentiated CD8 T cells, suggesting an enhanced CD8 maturation in patients who developed this toxicity (Figure 5G).

Patients with immune-related pneumonitis have distinctive distributions of T cell populations

Because pneumonitis is one of the most morbid complications of ICI treatment and our cohort included a relatively high proportion of patients who went on to develop this AE, we wondered whether distinct baseline T cell features might associate with

Figure 4. Selected subsets of CD4 helper T cells are associated with organ-specific irAEs

(A) Representative KNetL plot of cluster 14 and mean percentage differences in T_H $RORC^+$ $IL21^+$ cells per patient and across the disease groups: arthritis, pneumonitis, and thyroiditis.

(B) Subclustering of C14 cells into 6 sub clusters: sC1–sC6. Representative genes are shown separately.

(C) Heatmap showing the expression of markers associated with different subclusters among T_{H2} and T_{H17} families of cells. Black arrows indicate the subset defining markers.

(D) Differential clustering among the clinical irAE groups at baseline. Quantification of the percentages of cells in three clusters (sC3, sC4, and sC2) among irAE and no-irAE groups. The patients elected for each of the no-irAE groups were selected to match the type of underlying tumor.

(E) Correlation and RNA expression plots highlighting the association of candidate gene markers with T_{H2} and T_{H17}[23] clusters based on enrichment score. Representative KNetL plots showing the expression of candidate gene markers KLF6, S100B, and SIGLEC14 specifying the predictive cell populations present in pneumonitis and thyroiditis.

Statistical significance for unpaired comparisons was performed by Student's t test applying Mann-Whitney test. Data are presented as mean ± SEM. p value, exact, two-tailed, the center lines denote the mean of SEM. *$p < 0.05$, **$p < 0.01$, ***$p < 0.001$.

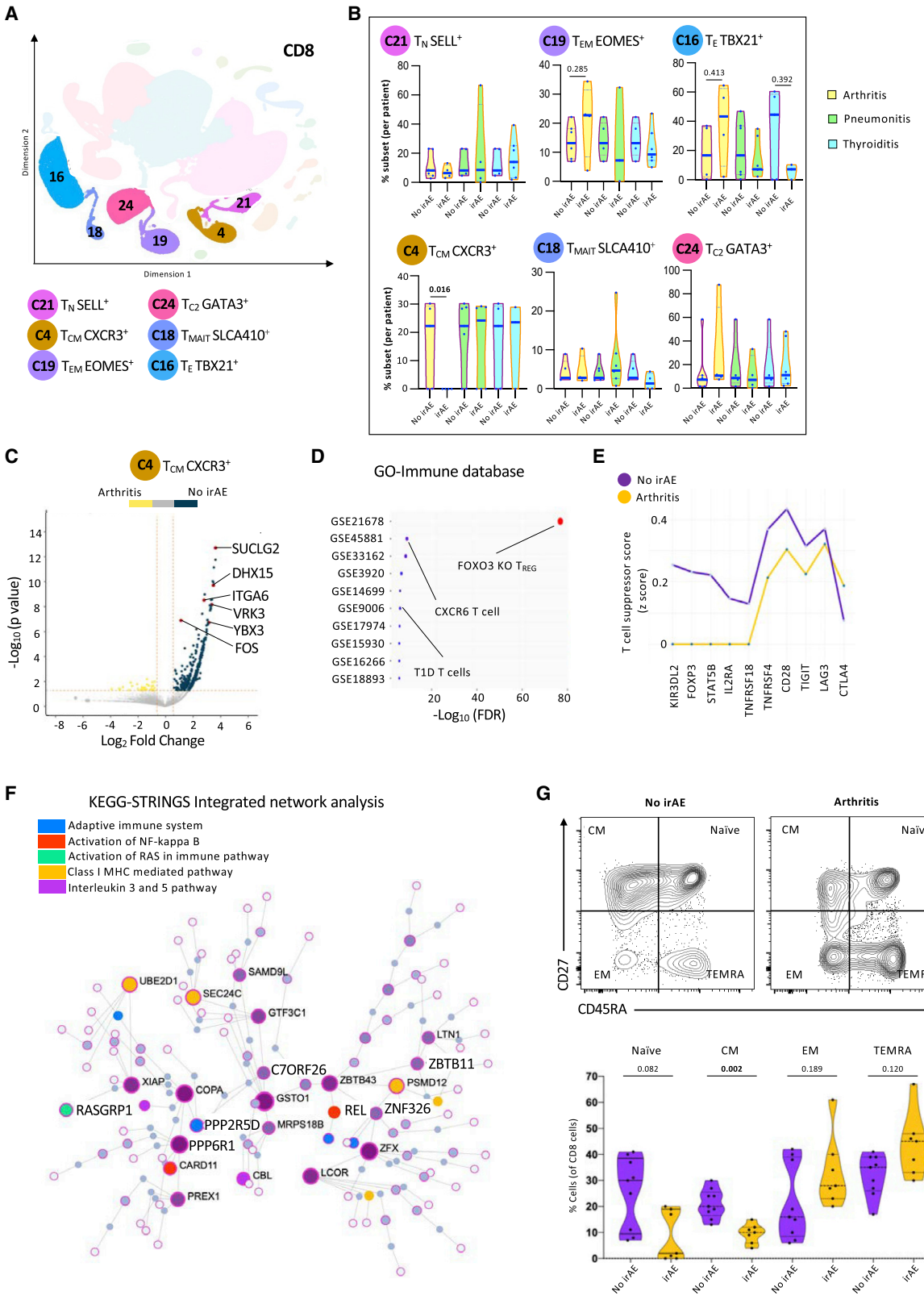

(legend on next page)

distinct subtypes of pneumonitis. Careful radiological analysis of serial chest computed tomography (CT) scans performed on the nine patients with pneumonitis (Figures S7A and S7B) revealed two clear subtypes: chronic hyperintensity pneumonitis (CHP), characterized by traction bronchiectasis and honeycombing, and organized pneumonia (OP), defined by patchy consolidation with a predominantly subpleural and peri-bronchial distribution (Figure 6A).[26] Moreover, the T cell cluster distribution (Figure 6B) of patients with CHP (Figure 6C) was distinct from that of patients with OP (Figure 6D). At baseline, unlike the patients with OP, patients with CHP had low levels of cells in clusters 4 (characterized by features of CD8 T_{CM} $CXCR3^+$ cells), 3 (double-positive T cells), and 10 (gamma delta T cells) and high levels of cells in clusters 22 (naïve-like CD4 T_N $TCF7^+LEF1^+$) and 25 (CD4 $T_{H1/2}$ $CXCR3^+GATA3^+$) (Figure 6E). Evaluation of the expression levels of genes exclusive to patients with CHP versus OP over the same subset of cells further supports the ability of this signature to differentiate between the two clinical presentations (Figure 6F). These findings suggest that the two types of pneumonitis were likely mediated by different populations of T cells. Moreover, this strong radiographical-immunological correlation supports the ability of scRNA-seq approach not just to annotate different subsets of T cells among patients with irAEs but also to uncover the potential contribution of specific T cell populations to clinical pathogenesis.

DISCUSSION

Immune checkpoints are T cell-surface-expressed inhibitory receptors that prevent excessive T cell responses. Tumor cells have evolved to usurp those inhibitory mechanisms to prevent T cell mediated tumor killing. Initially, the immune system recognizes and eliminates transformed cancerous cells prior to their development into tumors. However, during the process of carcinogenesis, tumor cells progressively express multiple inhibitory receptor ligands that will prevent T cell recognition. Consequently, therapeutic blockade of these checkpoints or their ligands with ICIs helps recover anti-tumor immunity. Since 2013, ICIs have been increasingly considered as targets for cancer immunotherapies due to the effectiveness of drugs blocking the inhibitory receptors CTLA-4, PD-1, and PD-L1.[27–30] The PD-1-PD-L1 interaction directly inhibits anti-tumor T cells, promotes peripheral T_E cell exhaustion, and supports the conversion of T_E cells into suppressive T_{REG} cells. Based on prolonged overall survival in clinical trials, Abs inhibiting PD-1 and PD-L1 have been approved for multiple clinical indications, including melanoma, non-small cell lung cancer, head and neck squamous cell carcinoma, urothelial carcinoma, renal cell carcinoma, Hodgkin's lymphoma, and other adult and pediatric solid tumors.

One in every two patients with cancer treated with ICIs targeting PD-1 will develop a side effect fitting within a spectrum termed irAEs. This broad array of inflammatory AEs affects different organ systems, including the skin, gastrointestinal tract, liver, endocrine organs, lungs, and joints. irAEs can develop at any time during the treatment, even months after discontinuing the treatment with the checkpoint blockade. The absence of predictive factors makes pre-treatment risk stratification extremely challenging on an individual patient level, as scant information exists to inform the type and severity of toxicity he or she may experience with treatment. Additionally, since the onset of irAEs is often sudden, and even fatal toxicities may occur, it is essential that clinicians recognize and manage the events early. The frequency of irAEs can be broken down by the type of ICIs received. A recent meta-analysis of irAE frequencies over multiple trials revealed that irAEs occurred in 74% of patients with cancer treated with anti-PD-1 or PD-L1 Abs; 89% of patients treated with anti-CTLA-4; 90% of patients receiving ICI combinations; and 89% of patients receiving ICIs with chemotherapy.[30] irAEs with grade 3 (severe) or grade 4 (life threatening) were reported in 14% of patients treated with PD-1 or PD-L1 inhibitors; 34% of patients treated with anti-CTLA-4 Abs; 55% of patients treated with ICI combinations; and 46% of patients treated with ICIs + chemotherapy agents. The rates of irAEs leading to treatment withdrawal were 6% after using the PD-1 or PD-L1 inhibitors; 21% for anti-CTLA-4 Abs; 38% for ICI combinations; and 13% for combinations with chemotherapy.

We identified that at baseline, patients with arthritis had significantly less cells with features of CD8 T_{CM} cells, patients with pneumonitis had more CD4 T_{H2} cells, and patients with thyroiditis had more CD4 T_{H17} cells when compared with patients who did not develop irAEs. These data support our hypothesis that different populations of T cells are associated with different irAEs and that quantification and characterization of these populations of T cell pre-treatment could serve as a toxicity-specific predictive biomarker. Quantification of these population of cells by means of larger studies using flow cytometry and RT-PCR are needed to further validate and translate our exploratory findings to the clinic.

In a previous study, gene expression profiling was performed on whole-blood samples from patients with melanoma to discover gene expression differences at baseline between

Figure 5. Patients with inflammatory arthritis have lower levels of central memory CD8 T cells at baseline

(A) Representative KNetL plot of annotated CD8 T cell clusters.

(B) Mean percentage of cells in six CD8 T cell subsets across the different clinical outcomes: arthritis, pneumonitis, and thyroiditis at baseline (unpaired t test).

(C) Volcano plot highlighting the up-regulated and down-regulated genes in T_{CM} $CXCR3^+$ cells in patients with no irAEs.

(D) GO analysis for differential genes present in T_{CM} $CXCR3^+$ cells from patients with no irAEs for enriched terms from Immune.MSigDB.

(E) Line graph showing the comparison of T cell states between cohorts of patients with no irAEs and arthritis based on the T suppressor cell signature score.

(F) Pathway analysis of differentially expressed genes in T_{CM} $CXCR3^+$ cells from patients with no irAEs using integrative KEGG-String platform.

(G) Quantification of flow cytometry data of 19 patients, showing percentages of naive, central memory (CM), effector memory (EM), and terminally differentiated T (TEMRA) cells at baseline.

Statistical significance for unpaired comparisons was performed by Student's t test applying Mann-Whitney test. Data are presented as mean ± SEM. p value, exact, two-tailed, the center lines denote the mean of SEM. *$p < 0.05$, **$p < 0.01$, ***$p < 0.001$.

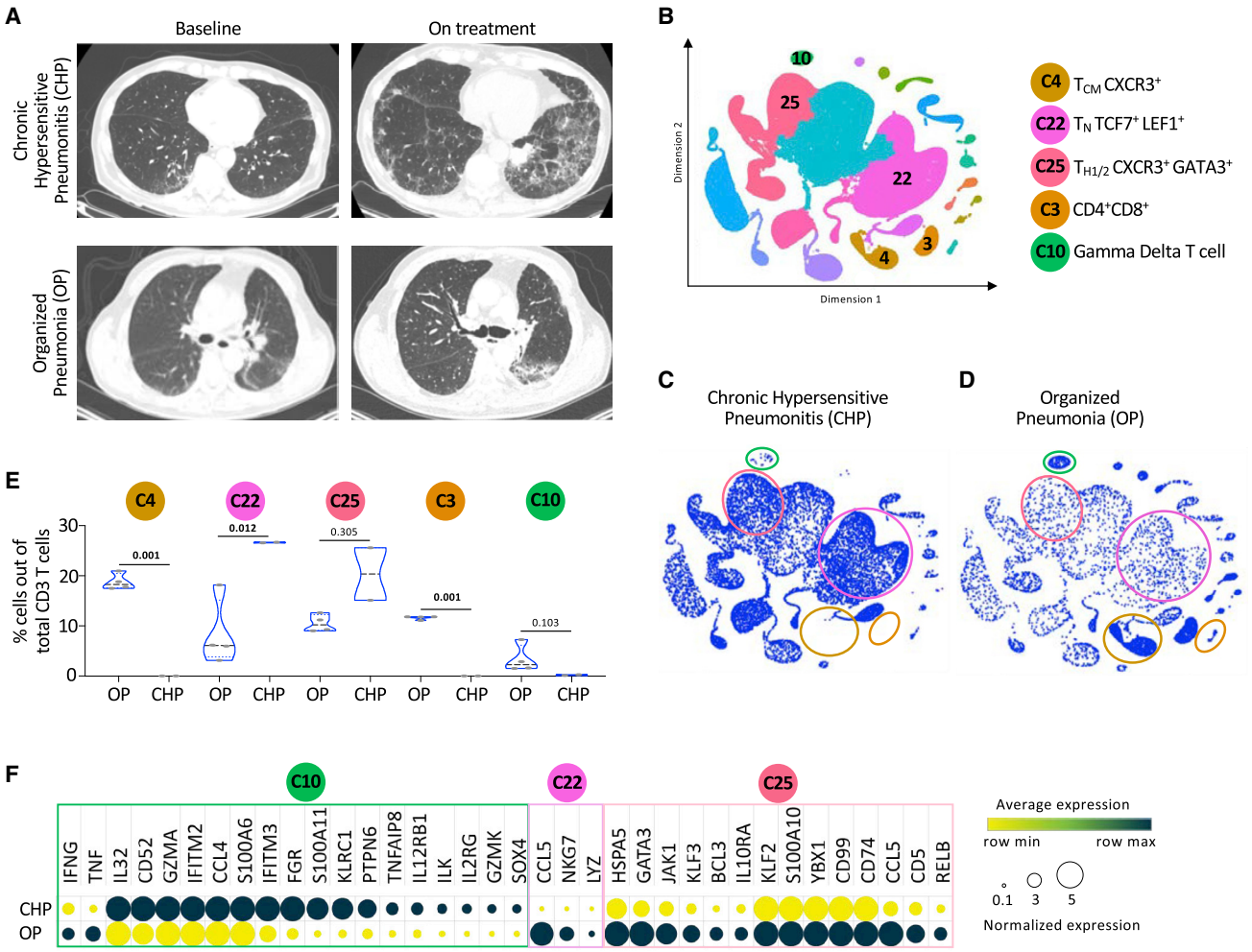

Figure 6. Patients with immune-related pneumonitis have distinctive distributions of T cell populations

(A) Representative chest CT scans of patients with chronic hypersensitive pneumonitis (CHP) and organized pneumonia (OP) at baseline and on treatment.

(B) Representative KNetL plot indicating key clusters to be used to distinguish the pneumonitis groups.

(C) Cells of patients with CHP are enriched in clusters C10, C3, and C4.

(D) Cells of patients with OP are depleted in clusters of C22 and C25.

(E) Quantification of the mean percentage differences in CD3 T cell subsets among the different pneumonitis groups.

(F) Heatmap showing the RNA expression of differentially expressed genes between CHP and OP groups within the clusters C10, C22, and C25.

Statistical significance for unpaired comparisons was performed by Student's t test applying Mann-Whitney test. Data are presented as mean ± SEM. p value, exact, two-tailed, the center lines denote the mean of SEM. *p < 0.05, **p < 0.01, ***p < 0.001.

patients who developed gastrointestinal toxicity following anti-CTLA-4 Ab treatment.[31] A more recent study documented T cell characteristics associated with irAEs in patients with melanoma using variety of single-cell technologies.[32] This study found that the pre-treatment levels of activated CD4 memory T cell and TCR diversity were associated with irAE development regardless of organ system involvement. This study complements our data and further support the concept that pre-treatment T cell characterization should predict irAE onset. This could be cancer-type dependent, where memory CD4 T cells are predictive in patients with melanoma while CD8 effecter T cells are associated with a lung cancer population. A recent work applied scRNA-seq to study peripheral blood samples from patients with melanoma treated with ICIs and discovered that pre-treatment-activated memory CD4 T cell abundance was associated with severe irAEs.[32] Another, more recent study analyzed peripheral blood from patients with arthritis irAEs and uncovered a correlation between the arthritis and a population of CD8 CX3CR1^{hi} T cells. Furthermore, and like our study, a subset of patients with irAEs had enhanced T_{H1} and T_{H17} gene signatures.[33] These studies, as well as our own work, support the concept that circulating T cells are associated with ICI-induced toxicity, with potential implications for improved diagnostics and clinical management.

To summarize, we discovered correlations between the presence of specific subsets of T cells at baseline and the

development of arthritis, pneumonitis, and thyroiditis AEs. These exciting findings suggest that quantification of these populations of T cells before the treatment has the potential to predict who will develop irAEs and position the clinical team to initiate earlier immunomodulatory therapy. The ability to predict irAEs is critically important to improve the effectiveness and the usability of cancer immunotherapies. Through our ongoing efforts, we will translate our findings to the clinic by developing a personalized flow cytometry- and RT-PCR-based tool to prove the premise that quantification of these population of cells could accurately predict irAEs, altogether enabling many more patients with cancer to safely receive immunotherapies.

Limitations of the study

Our study is not free of limitations.[34] One limitation is the fact that this was a single-center, retrospective, case control study of 40 patients, and the incidence and types of irAEs in our institute might be different from other locations. Another limitation is the relatively small number of patients with each type of irAE. With these numbers, we discovered T cell populations and subsets that were associated with specific irAEs. In order to validate these subsets of T cells as a biomarker to predict irAEs, additional patients must be recruited. One of the interesting findings of our study was the lack of differences in naive, T_H, or T_E cell population percentages between the patients that were treated with anti-PD-1 or anti-PD-L1. On the one hand, this is not unexpected since the type, incidence, and severity of irAEs are similar between these groups. On the other hand, it is unlikely that these drugs utilize the same molecular mechanism to trigger irAEs.

STAR★METHODS

Detailed methods are provided in the online version of this paper and include the following:

- KEY RESOURCES TABLE
- RESOURCE AVAILABILITY
  - Lead contact
  - Materials availability
  - Data and code availability
- EXPERIMENTAL MODEL AND SUBJECT DETAILS
- METHOD DETAILS
  - Patient recruitment
  - General reagents
  - Cell isolation and preparation for sequencing
  - Data analysis
  - Flow cytometry
  - CT scan
- QUANTIFICATION AND STATISTICAL ANALYSIS

SUPPLEMENTAL INFORMATION

Supplemental information can be found online at https://doi.org/10.1016/j.xcrm.2022.100868.

ACKNOWLEDGMENTS

We would like to acknowledge Dr. Michael Peled and Dr. Jair Bar (Tel Aviv University) for providing blood samples and Dr. Faizan Danish for assisting with the statistical analysis. We would like to thank the expertise and assistance of Darwin D'Souza and Travis Dawson of the Human Immune Monitoring Center (HIMC) at Mount Sinai Icahn School of Medicine. This work was supported by grants from the NIH (AI125640, CA231277, and AI150597); the Cancer Research Institute; the Lisa Baker Autoimmunity Innovation Fund; and the V Foundation. We would like to thank the Genome Technology Center (GTC) for expert library preparation and sequencing and the Applied Bioinformatics Laboratories (ABL) for providing bioinformatics support and helping with the analysis and interpretation of the data. The GTC and ABL are shared resources partially supported by Cancer Center Support Grant P30CA016087 at the Laura and Isaac Perlmutter Cancer Center. This work has used computing resources at the NYU School of Medicine High Performance Computing (HPC) Facility. Research reported in this publication was also performed in the CCTI Flow Cytometry Core, supported in part by the Office of the Director, National Institutes of Health under awards S10RR027050 and S10OD020056.

AUTHOR CONTRIBUTIONS

Conception and design, S.B., N.R., and A.M.; development of methodology, S.B., K.A., R.J.W., A.T., S.L., and A.M.; acquisition of data, S.B., R.M., S.L.R., and A.M.; analysis and interpretation of data, S.B., R.J.W., Z.L., A.K.-J., A.T., G.G.L., M.M.S., and A.M.; writing – review and/or revision of the manuscript, S.B. and A.M.; technical or material support, B.S.H., M.M.S., G.G.L., M.C.D., M.M., N.R., M.S., and K.A.; study supervision, B.S.H. and A.M.

DECLARATION OF INTERESTS

The authors declare no competing interests.

Received: March 14, 2022
Revised: July 13, 2022
Accepted: November 22, 2022
Published: December 12, 2022

REFERENCES

1. Hamid, O., Robert, C., Daud, A., Hodi, F.S., Hwu, W.-J., Kefford, R., Wolchok, J.D., Hersey, P., Joseph, R.W., Weber, J.S., and Ribas, A. (2013). Safety and tumor responses with lambrolizumab (Anti–PD-1) in melanoma. N. Engl. J. Med. *369*, 134–144.
2. Rizvi, N.A., Mazières, J., Planchard, D., Stinchcombe, T.E., Dy, G.K., Antonia, S.J., Horn, L., Lena, H., Minenza, E., Mennecier, B., et al. (2015). Activity and safety of nivolumab, an anti-PD-1 immune checkpoint inhibitor, for patients with advanced, refractory squamous non-small-cell lung cancer (CheckMate 063): a phase 2, single-arm trial. Lancet Oncol. *16*, 257–265. https://doi.org/10.1016/S1470-2045(15)70054-9.
3. Hodi, F.S., O'Day, S.J., McDermott, D.F., Weber, R.W., Sosman, J.A., Haanen, J.B., Gonzalez, R., Robert, C., Schadendorf, D., Hassel, J.C., et al. (2010). Improved survival with ipilimumab in patients with metastatic melanoma. N. Engl. J. Med. *363*, 711–723.
4. Postow, M.A., Chesney, J., Pavlick, A.C., Robert, C., Grossmann, K., McDermott, D., Linette, G.P., Meyer, N., Giguere, J.K., Agarwala, S.S., et al. (2015). Nivolumab and ipilimumab versus ipilimumab in untreated melanoma. N. Engl. J. Med. *372*, 2006–2017.
5. Weber, J.S., D'Angelo, S.P., Minor, D., Hodi, F.S., Gutzmer, R., Neyns, B., Hoeller, C., Khushalani, N.I., Miller, W.H., Jr., Lao, C.D., et al. (2015). Nivolumab versus chemotherapy in patients with advanced melanoma who progressed after anti-CTLA-4 treatment (CheckMate 037): a randomised, controlled, open-label, phase 3 trial. Lancet Oncol. *16*, 375–384.
6. Borcoman, E., Kanjanapan, Y., Champiat, S., Kato, S., Servois, V., Kurzrock, R., Goel, S., Bedard, P., and Le Tourneau, C. (2019). Novel patterns of response under immunotherapy. Ann. Oncol. *30*, 385–396.
7. de Miguel, M., and Calvo, E. (2020). Clinical challenges of immune checkpoint inhibitors. Cancer Cell *38*, 326–333.

8. Postow, M.A., Sidlow, R., and Hellmann, M.D. (2018). Immune-related adverse events associated with immune checkpoint blockade. N. Engl. J. Med. *378*, 158–168.

9. Dolladille, C., Ederhy, S., Sassier, M., Cautela, J., Thuny, F., Cohen, A.A., Fedrizzi, S., Chrétien, B., Da-Silva, A., Plane, A.F., et al. (2020). Immune checkpoint inhibitor rechallenge after immune-related adverse events in patients with cancer. JAMA Oncol. *6*, 865–871.

10. Chang, C.Y., Park, H., Malone, D.C., Wang, C.Y., Wilson, D.L., Yeh, Y.M., Van Boemmel-Wegmann, S., and Lo-Ciganic, W.H. (2020). Immune checkpoint inhibitors and immune-related adverse events in patients with advanced melanoma: a systematic review and network meta-analysis. JAMA Netw. Open *3*. e201611.

11. Martins, F., Sofiya, L., Sykiotis, G.P., Lamine, F., Maillard, M., Fraga, M., Shabafrouz, K., Ribi, C., Cairoli, A., Guex-Crosier, Y., et al. (2019). Adverse effects of immune-checkpoint inhibitors: epidemiology, management and surveillance. Nat. Rev. Clin. Oncol. *16*, 563–580.

12. Da, L., Teng, Y., Wang, N., Zaguirre, K., Liu, Y., Qi, Y., and Song, F. (2019). Organ-specific immune-related adverse events associated with immune checkpoint inhibitor monotherapy versus combination therapy in cancer: a meta-analysis of randomized controlled trials. Front. Pharmacol. *10*, 1671.

13. Oh, D.Y., Cham, J., Zhang, L., Fong, G., Kwek, S.S., Klinger, M., Faham, M., and Fong, L. (2017). Immune toxicities elicted by CTLA-4 blockade in cancer patients are associated with early diversification of the T-cell repertoire. Cancer Res. *77*, 1322–1330.

14. Yasuda, Y., Iwama, S., Sugiyama, D., Okuji, T., Kobayashi, T., Ito, M., Okada, N., Enomoto, A., Ito, S., Yan, Y., et al. (2021). CD4$^+$ T cells are essential for the development of destructive thyroiditis induced by anti-PD-1 antibody in thyroglobulin-immunized mice. Sci. Transl. Med. *13*. eabb7495.

15. Tang, K.H., Li, S., Khodadadi-Jamayran, A., Jen, J., Han, H., Guidry, K., Chen, T., Hao, Y., Fedele, C., Zebala, J.A., et al. (2021). Combined inhibition of SHP2 and CXCR1/2 promotes antitumor T-cell response in NSCLC. Cancer Discov. *12*, 47–61. https://doi.org/10.1158/2159-8290.CD-21-0369.

16. Ho, I.C., Tai, T.S., and Pai, S.Y. (2009). GATA3 and the T-cell lineage: essential functions before and after T-helper-2-cell differentiation. Nat. Rev. Immunol. *9*, 125–135.

17. Singh, S.S., Chauhan, S.B., Ng, S.S., Corvino, D., de Labastida Rivera, F., Engel, J.A., Waddell, N., Mukhopadhay, P., Johnston, R.L., Koufariotis, L.T., et al. (2022). Increased amphiregulin expression by CD4$^+$ T cells from individuals with asymptomatic *Leishmania donovani*infection. Clin. Transl. Immunology *11*. e1396.

18. García-Sánchez, A., Estravís, M., Martin, M.J., Pérez-Pazos, J., Martín-García, C., Gil-Melcón, M., Ramos-González, J., Eguiluz-Gracia, I., Triviño, J.C., Isidoro-García, M., et al. (2021). *PTGDR2* expression in peripheral blood as a potential biomarker in adult patients with asthma. J. Pers. Med. *11*, 827.

19. Koetzier, S.C., van Langelaar, J., Wierenga-Wolf, A.F., Melief, M.J., Pol, K., Musters, S., Lubberts, E., Dik, W.A., Smolders, J., and van Luijn, M.M. (2022). Improving glucocorticoid sensitivity of brain-homing CD4$^+$ T helper cells by steroid hormone crosstalk. Front. Immunol. *13*. 893702.

20. Lam, A.J., Lin, D.T.S., Gillies, J.K., Uday, P., Pesenacker, A.M., Kobor, M.S., and Levings, M.K. (2021). Optimized CRISPR-mediated gene knockin reveals FOXP3-independent maintenance of human Treg identity. Cell Rep. *36*. 109494.

21. Lee, Y., Awasthi, A., Yosef, N., Quintana, F.J., Xiao, S., Peters, A., Wu, C., Kleinewietfeld, M., Kunder, S., Hafler, D.A., et al. (2012). Induction and molecular signature of pathogenic TH17 cells. Nat. Immunol. *13*, 991–999.

22. Gaublomme, J.T., Yosef, N., Lee, Y., Gertner, R.S., Yang, L.V., Wu, C., Pandolfi, P.P., Mak, T., Satija, R., Shalek, A.K., et al. (2015). Single-cell genomics unveils critical regulators of Th17 cell pathogenicity. Cell *163*, 1400–1412. https://doi.org/10.1016/j.cell.2015.11.009.

23. Tirosh, I., Izar, B., Prakadan, S.M., Wadsworth, M.H., 2nd, Treacy, D., Trombetta, J.J., Rotem, A., Rodman, C., Lian, C., Murphy, G., et al. (2016). Dissecting the multicellular ecosystem of metastatic melanoma by single-cell RNA-seq. Science *352*, 189–196.

24. Selleri, S., Deola, S., Pos, Z., Jin, P., Worschech, A., Slezak, S.L., Rumio, C., Panelli, M.C., Maric, D., Stroncek, D.F., et al. (2008 Apr 15). GM-CSF/IL-3/IL-5 receptor common beta chain (CD131) expression as a biomarker of antigen-stimulated CD8+ T cells. J. Transl. Med. *6*, 17.

25. Sasaki, K., Moussawy, M.A., Abou-Daya, K.I., Macedo, C., Hosni-Ahmed, A., Liu, S., Juya, M., Zahorchak, A.F., Metes, D.M., Thomson, A.W., et al. (2022). Activated-memory T cells influence naïve T cell fate: a noncytotoxic function of human CD8 T cells. Commun. Biol. *5*, 634.

26. Raghu, G., and Meyer, K.C. (2021). Cryptogenic organising pneumonia: current understanding of an enigmatic lung disease. Eur. Respir. Rev. *30*. 210094.

27. Hayashi, H., and Nakagawa, K. (2020). Combination therapy with PD-1 or PD-L1 inhibitors for cancer. Int. J. Clin. Oncol. *25*, 818–830.

28. Mahoney, K.M., Freeman, G.J., and McDermott, D.F. (2015). The next immune-checkpoint inhibitors: PD-1/PD-L1 blockade in melanoma. Clin. Ther. *37*, 764–782.

29. Gide, T.N., Quek, C., Menzies, A.M., Tasker, A.T., Shang, P., Holst, J., Madore, J., Lim, S.Y., Velickovic, R., Wongchenko, M., et al. (2019). Distinct immune cell populations define response to anti-PD-1 monotherapy and anti-PD-1/anti-CTLA-4 combined therapy. Cancer Cell *35*, 238–255.e6.

30. Hussaini, S., Chehade, R., Boldt, R.G., Raphael, J., Blanchette, P., Maleki Vareki, S., and Fernandes, R. (2021). Association between immune-related side effects and efficacy and benefit of immune checkpoint inhibitors - a systematic review and meta-analysis. Cancer Treat Rev. *92*. 102134.

31. Shahabi, V., Berman, D., Chasalow, S.D., Wang, L., Tsuchihashi, Z., Hu, B., Panting, L., Jure-Kunkel, M., and Ji, R.R. (2013). Gene expression profiling of whole blood in ipilimumab-treated patients for identification of potential biomarkers of immune-related gastrointestinal adverse events. J. Transl. Med. *11*, 75.

32. Lozano, A.X., Chaudhuri, A.A., Nene, A., Bacchiocchi, A., Earland, N., Vesely, M.D., Usmani, A., Turner, B.E., Steen, C.B., Luca, B.A., et al. (2022). T cell characteristics associated with toxicity to immune checkpoint blockade in patients with melanoma. Nat. Med. *28*, 353–362. https://doi.org/10.1038/s41591-021-01623-z.

33. Kim, S.T., Chu, Y., Misoi, M., Suarez-Almazor, M.E., Tayar, J.H., Lu, H., Buni, M., Kramer, J., Rodriguez, E., Hussain, Z., et al. (2022). Distinct molecular and immune hallmarks of inflammatory arthritis induced by immune checkpoint inhibitors for cancer therapy. Nat. Commun. *13*, 1970.

34. Mor, A., and Strazza, M. (2021). Bridging the gap: connecting the mechanisms of immune-related adverse events and autoimmunity through PD-1. Front. Cell Dev. Biol. *9*. 790386.

STAR★METHODS

KEY RESOURCES TABLE

REAGENT or RESOURCE	SOURCE	IDENTIFIER
Antibodies		
APC/Cyanine7 anti-human CD3 (clone HIT3A)	BioLegend	Cat# 300318; RRID: AB_314054
Alexa Fluor® 700 anti-human CD4 (clone RPA-T4)	BioLegend	Cat# 300526; RRID: AB_493743
PE/Cyanine7 anti-human CD8a (clone RPA-T8)	BioLegend	Cat# 301012; RRID: AB_314130
Brilliant Violet 605™ anti-human CD45RA (clone HI100)	BioLegend	Cat# 304134; RRID: AB_11126164
Alexa Fluor® 488 anti-human CD27 Recombinant antibody	BioLegend	Cat# 393204; RRID: AB_2750088
BD Horizon™ BUV496 Mouse Anti-Human CD8	BD Biosciences	Cat# 612942; RRID: AB_2870223
BD Horizon™ BUV805 Mouse Anti-Human CD3	BD Biosciences	Cat# 612895; RRID: AB_2870183
BD Horizon™ BV750 Mouse Anti-Human CD4	BD Biosciences	Cat# 566355; RRID: AB_2744426
BD OptiBuild™ BUV395 Mouse Anti-Human CD45RA	BD Biosciences	Cat# 740298; RRID: AB_2740037
BD Horizon™ BV786 Rat Anti-Human CCR7 (CD197)	BD Biosciences	Cat# 563710; RRID: AB_2738384
CITEseq antibodies		
TotalSeq™-C0072 anti-human CD4 Antibody	BioLegend	Cat# 300567; RRID: AB_2800725
TotalSeq™-C0046 anti-human CD8 Antibody	BioLegend	Cat# 344753; RRID: AB_2800922
TotalSeq™-C0154 anti-human CD27 Antibody	BioLegend	Cat# 302853; RRID: AB_2800747
TotalSeq™-C0063 anti-human CD45RA Antibody	BioLegend	Cat# 304163; RRID: AB_2800747
Chemicals, peptides, and recombinant proteins		
DNase I	STEMCELL Technologies	Cat# 7470
Zombie UV™ Fixable Viability Kit	BioLegend	Cat# 423107
Critical commercial assays		
Chromium Single Cell 5′ Library & Gel Bead Kit	10x Genomics	Cat# 1000006
RNA Isolation Kit	Qiagen	Cat# 74104
Software and algorithms		
FlowJo 10.1r7	https://www.flowjo.com	SCR_008520
Single cell RNAseq analysis	https://github.com/rezakj/iCellR	N/A
GraphPad Prism 9	https://www.graphpad.com	SCR_002798
InnateDB	https://www.innatedb.com	SCR_006714
ShinyGO v0.76	http://bioinformatics.sdstate.edu/go	SCR_019213
Enrichr	https://maayanlab.cloud/Enrichr	SCR_001575
Cell Ranger	https://support.10xgenomics.com/single-cell-vdj/software/pipelines/latest/what-is-cell-ranger	SCR_017344
Deposited data		
RNA sequencing data	https://www.ncbi.nlm.nih.gov/geo	GSE159774

RESOURCE AVAILABILITY

Lead contact

Further information and requests for resources and reagents should be direct to and will be fulfilled by the lead contact, Adam Mor, M.D., Ph.D. (am5121@cumc.columbia.edu).

Materials availability

This study did not generate new unique reagents.

Data and code availability

Datasets generated in this study have been uploaded to GEO database: accession number GSE216329. This study reports original code: https://github.com/rezakj/iCellR. Any additional information required to reanalyze the data reported in this study is available from the lead contact upon request.

EXPERIMENTAL MODEL AND SUBJECT DETAILS

The expedient model in this work was limited to human subjects. The average age of the patients was 70 years old, 45% were males and 55% were females. All the patients were diagnosed with solid malignancies and were treated with immune checkpoint inhibits in our institute. This study protocol was approved and oversighted by our institute (IRB protocol IRB#AAA-O5706).

METHOD DETAILS

Patient recruitment

We collected blood from cancer patients prior to anti-PD-1 therapy (Nivolumab or Pembrolizumab), anti-PD-L1 (Atezolizumab), and anti-CTLA-4 (Ipilimumab) initiation and at the time of irAEs onset according to our experimental workflow (Figure 1). Twenty-four immunotherapy-naïve cancer patients were consented according to IRB protocol IRB#AAA-O5706/L5871. We collected information about treatment regimens, duration of therapy, progression-free survival, and overall survival for all patients. We additionally collected information on documented irAE emergence and treatment. Inclusion criteria included histologically confirmed cancer, immunotherapy-naïve, and planned initiation of immunotherapy as an immediate next step in therapy. Major exclusion criteria were active infection, history of autoimmune disease, immune suppressive therapy, active pneumonitis or pulmonary fibrosis, or recent administration of live-virus vaccines. We collected 10 mL of blood from each patient in EDTA vacutainers prior to initiation of the treatment. Additional 10 mL peripheral blood were collected at the time of first irAEs presentation. For our control group, cancer patients who did not develop irAEs, the timing of the second blood collection was matched to the number of weeks following anti-PD-1 therapy initiation at which blood was collected from the irAEs patients.

General reagents

RPMI 1640 medium, Dulbecco's PBS, and FBS were purchased from Life Technologies.

Cell isolation and preparation for sequencing

Red blood cells were lysed by resuspending cell pellets in ACK Lysis Buffer (Gibco) for 2 min, followed by washing with cold PBS. We used RosetteSep T cell enrichment kit (StemCell) to isolate untouched CD3 T cells. Each sample was washed once with RPMI and 3 times with PBS +2% BSA before labeling and pooling. Specimens were then filtered through 70 um strainers (Fisher). Cell concentration, singularity, and viability were confirmed with a hematocytometer before submission for scRNA-Seq (10X Genomics). Cells were processed for scRNAseq by employing CITEseq methodology using multiplexed cell surface markers using labeled with a cocktail of oligonucleotide tagged Total-Seq anti-human antibodies (BioLegend) against CD4, CD8, CD45RA and CD27. 17,000 antibody labeled cells, from each sample, were loaded on Chromium microfluidics chip for single cell/gel bead encapsulation, barcoding and reverse transcription according to the manufacturer's recommendations. After cDNA amplification, <180bp nucleotide fragments containing antibody-derived tags (ADTs) and >300bp nucleotide fragments containing mRNA-derived cDNA will be size separated as previously described. 5′ single cell sequencing library was generated using a tagmentation-based approach and according to manufacturer's recommendations. ADTs and cDNA libraries were merged and subjected to Illumina 150bp paired-end sequencing.

Data analysis

Quality controls included calculation of the number of genes, UMIs, and the proportion of mitochondrial genes for each cell. Cells with a low number of covered genes (gene-count <500) or high mitochondrial counts (mt-genes >0.2) were filtered out, and the matrix was normalized based on library size. A general statistical test was performed to calculate gene dispersion, base mean, and cell coverage. iCellR, an R package (v1.5.5) (https://CRAN.R-project.org/package=iCellR) and genes with high dispersion and coverage (2000 genes) were used to perform Principal Component Analysis (PCA) and batch alignment. Uniform Manifold Approximation and Projection (UMAP) and K-nearest-neighbor-based Network graph drawing Layout (KNetL) were then performed. KNetL map has a zoom option which allowed us to see variable levels of detail (more or fewer sub-populations in cell communities). In the study, we used a zoom of 500. The network layout used in KNetL map was force-based, and the zoom option changed the force in the system. Force-directed graph drawing algorithms assign attractive (analogous to spring force) and repulsive forces (usually described as analogous to the forces in atomic particles) to separate all pairs of nodes. PhenoGraph clustering was then performed on the KNetL map results, and marker genes were found for each cluster and visualized on heatmaps, bar plots, and boxplots as indicate. Marker genes were then used to assign cell types. Imputation was used for data visualizations only and not for the analysis. Signature enrichment scoring was generated by calculating z-scores relative to naive T cells or by the scoring method described by Tirosh et al.,[32] using i.score function on the main data. Gene Ontology analysis of immune cell

signatures and disease catalogs were collectively performed using innateDB (https://www.innatedb.com), ShinyGO v0.76 (http://bioinformatics.sdstate.edu/go) and Enrichr (https://maayanlab.cloud/Enrichr). Overlayed network analysis and pathway analysis was performed by innateDB (https://www.innatedb.com).

Flow cytometry

For protein expression analysis following isolation cells were collected and stained with the following antibodies for surface protein expression: CD3 APC-Cy7 (BioLegend), CD4 AF-700 (BioLegend), CD8 PE-Cy7 (BioLegend), CD45RA BV-605 (BioLegend), CD27 AF-488 (BioLegend), CD8 BUV-496 (BD Biosciences), CD3 BUV-805 (BD Biosciences), CD4 BV-750 (BD Biosciences), CD45RA BUV-395 (BD Biosciences), and CCR7 BV-786 (BD Biosciences). Dead cells were excluded from the analysis by using Zombie-UV (Biolegend). Doublets and double-positive CD4/CD8 cells were removed through sequential gating. Flow cytometry acquisition was done using the BD LSRII with BD FACSDiva. Data was analyzed by FlowJo 10.1r7 and GraphPad Prism 9.

CT scan

Computed-tomography scans were performed per standard of care before and during immunotherapy administration. Scans from patients who experienced pneumonitis were reviewed and annotated by an experienced thoracic radiologist.

QUANTIFICATION AND STATISTICAL ANALYSIS

Unless otherwise specified, the data are presented as mean ± standard error of the mean. Statistical significance was determined using Student's *t* test, 1-way ANOVA, or log rank test, as indicated. Statistical analyses were performed using Prism 9 (GraphPad Software). Significance was set at $p = 0.05$. To measure the variance between each patient at baseline to on treatment condition, un-paired non-parametric test was applied wherever indicated. To compute the correlation between signature enrichment scores, a non-parametric spearman correlation was applied choosing two-tailed p value with a confidence interval of 95%, where indicated. For this observational study, our sample size calculation of $n = 24$ subjects per time point was based on published RNA-seq data assuming that the average read count among the prognostic genes in the control group is 100, the maximum dispersion is 0.15, and the ratio of the geometric mean of normalization factors is 1. Our minimum effect size was 2 and we were able to reject the null hypothesis that the population means of the two groups are equal with an estimated power of 0.98. The FDR associated with this test is 0.01.

Cell Reports Medicine, Volume *4*

Supplemental information

Single-cell RNA sequencing reveals distinct T cell populations in immune-related adverse events of checkpoint inhibitors

Shoiab Bukhari, Brian S. Henick, Robert J. Winchester, Shalom Lerrer, Kieran Adam, Yevgeniya Gartshteyn, Rohan Maniar, Ziyan Lin, Alireza Khodadadi-Jamayran, Aristotelis Tsirigos, Mary M. Salvatore, Galina G. Lagos, Steven L. Reiner, Matthew C. Dallos, Matthen Mathew, Naiyer A. Rizvi, and Adam Mor

A

Patient Key	Clinical	Age	Gender	Tumor	Stage	irAE type	irAE grade	Steroids	Weeks to onset
P1	Arthritis	49	Female	NSCLC	4	Musculoskeletal	3	Systemic	4-6
P2	Arthritis	62	Female	NSCLC	4	Musculoskeletal	2	Systemic	4-6
P3	Arthritis	53	Female	NSCLC	3	Musculoskeletal	2	Intra-articular	4-6
P4	Thyroditis	73	Male	NSCLC	4	Endocrine	3	None	N/A
P5	Thyroiditis	70	Male	NSCLC	4	Endocrine	3	None	N/A
P6	Thyroiditis	76	Male	NSCLC	4	Endocrine-Renal	2	Systemic	N/A
P7	Arthritis	65	Female	NSCLC	4	Musculoskeletal	2	Systemic	4-6
P8	Pneumonitis	75	Male	NSCLC	4	Pulmonary	2	Systemic	4-6
P9	no irAE	75	Female	NSCLC	4	none	0		No irAE
P10	Pneumonitis	51	Female	NSCLC	4	Pulmonary	3	Systemic	4-6
P11	Pneumonitis	55	Male	NSCLC	4	Pulmonary	2	Systemic	4-6
P12	Pneumonitis	72	Male	NSCLC	4	Pulmonary	2	Systemic	4-6
P13	Pneumonitis	58	Male	Prostate	N/A	Pulmonary	3	Systemic	4-6
P14	Pneumonitis	74	Male	Prostate	N/A	Pulmonary	3	Systemic	4-6
P15	Pneumonitis	52	Female	NSCLC	4	Pulmonary-Endocrine-Renal	3	Systemic	4-6
P16	Neuritis	65	Female	NSCLC	4	Neuro-Gastrointestinal	3	Systemic	
P17	no irAE	67	Male	NSCLC	4	none	0	None	No irAE
P18	no irAE	40	Female	HNSCC	4	none	0	None	No irAE
P19	no irAE	74	Male	HNSCC	4	none	0	None	No irAE
P20	no irAE	77	Male	NSCLC	4	none	0	None	No irAE
P21	no irAE	81	Male	NSCLC	4	none	0	None	No irAE
P22	no irAE	68	Female	NSCLC	4	none	0	None	No irAE
P23	no irAE	69	Male	Prostate	N/A	none	0	None	No irAE
P24	no irAE	66	Male	Prostate	N/A	none	0	None	No irAE

B

Patients	irAEs group	
Age (average)		70 years
Gender (n)	Male	62
	Female	73
Tumor type	Lung	46
	GU	37
	Melanoma	25
	Other	27
Agent (ICIs)	Pembrolizumab	28
	Nivolumab	41
	Atezolizumab	21
	Durvalumab	2
	Combination	43
irAEs type	Joints	58
	Skin	16
	Neurologic	16
	Endocrine	20
	Pulmonary	14
	Other	26
irAEs grade		2.7
Time to onset		57 days
Total number of patients		**135**

Table S1. Clinical characterization of the patients enrolled to the study, related to figure 1.

CD8+ T cells annotation				CD4+ T cells annotation			
Subset	Surface Markers	Intracellular/Transcription factors	Cytokines	Subset	Surface Markers	Intracellular/Transcription factors	Cytokines
Naïve	SELL			**TH1**	KLRD1	STAT1	TNF
	IL7R				IFNGR1	STAT4	LTA
	CCR7				CXCR3	TBX21	IFNG
	CD45RA				CXCR6		IL2
	CD27				CCR1		
					CCR5		
Effector	IL2RA	TBX21	IFNG		IL12RB1		
	TNFRSF8		IL2		IL18R1		
	CD69		PRF1		TNFSF11		
	TNFRSF4		GZMB / GZMA		HAVCR2		
	ICOS		TNFA				
	KLRG1		CCL3				
	HAVCR2		CCL4	**TH2**	CXCR4	BATF	IL4
			CCL5		CCR4	GATA3	IL5
					CCR8	IRF4	IL13
					PTGDR2	STAT6	AREG
					HAVCR1		
Effector Memory	CD44	EOMES	GZMK		IL17RB		
	CD45RO /CD45RA-	TBET	IFNG++		IL33		
	CD62L low		TNFA++				
	CD127 high		PRF1				
	KLRG1 high		IL2				
	CCR7 low			**TH17**	IL1R1	AHR	CSF2
					KLRB1	BATF	IL17A
					CCR4	MAF	IL17AF
Central Memory	CD45RO/CD45 RA-	TBET	IFNG		CCR6	NFKBIZ	IL17F
	CD62L low	EOMES	IL2		IL21R	IRF4	IL21
	CD127 ++		TNFA		IL12RB1	RORA	IL22
	CCR7 low					RORC	
	CD27					STAT3	
	CD28						
	CXCR3 mid			**CD4 Cytotoxic**		TBX21	PRF1
							GZMB
MAIT cells	KLRB1	SLC4A1					GZMA
		ZBTB16					
				TREG	CTLA4	FOXP3	
Regulatory	CD57	B3GAT1			IL2RA		
	CD28-	FOXP3					
	KLRG1++	IKAROS					
	PD1	EGR1		**TFH**	CXCR3	BATF	IL21
	LAG3	EGR2			CXCR5	BCL6	
	HLADR				ICOS	MAF	
					PDCD1	IFR4	
						STAT3	
TRMs	CD69+	ITGA1					
	CD103+/-	ITGAE					
	CD101	SELPLG					
	CD49a	Hobit					
	PD1	Blimp1					
	CXCR6	Runx3					
	CLA	Notch/RBPj					
	CCR8						

Table S2. T cell subset markers, related to figure 2.

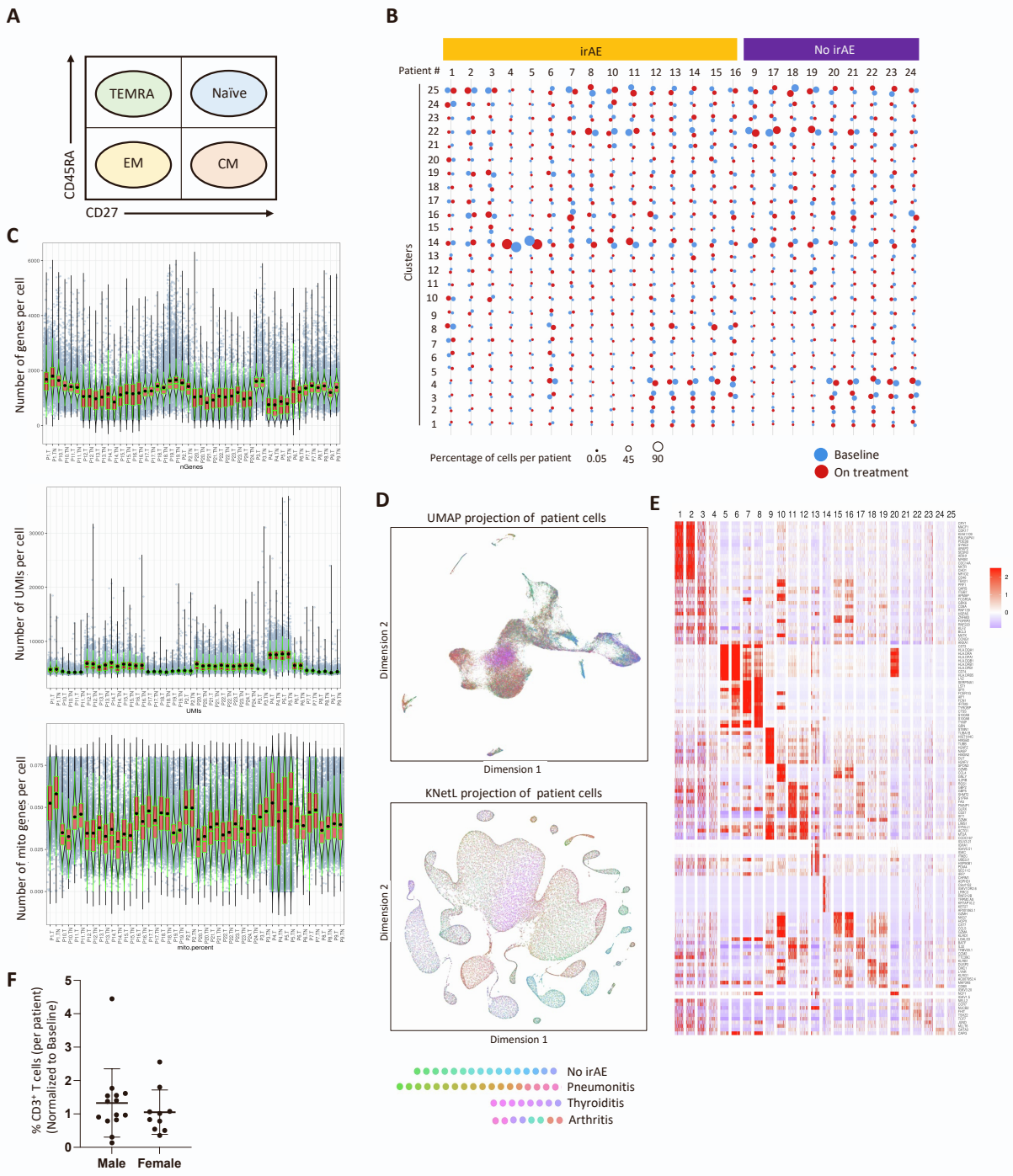

Supplemental figure 1. T cells annotation and characterization, related to figure 2. (A) T cells were annotated into Naïve, central memory (CM), effector memory (EM), terminally differentiated (TEMRA) maturation subsets based on expression levels of CD27 and CD45RA. (B) Qualitative representation of T cell abundances at baseline and on treatment within each cluster per patient using Beeswarm map. (C) Quality control bar plots showing the number of genes, UMI, mito genes per cell. (D) UMAP and KNetL projection of cells contributed by each patient. (E) Heatmap representation of cluster defining marker genes and other cluster associated genes. (F) Dot plot representing the total T cell distribution in males compared to females. Statistical significance: T test, unpaired Mann-Whitney, P-value, Exact-two-tailed, the center lines denote the mean of SEM. T (on treatment) TN (baseline).

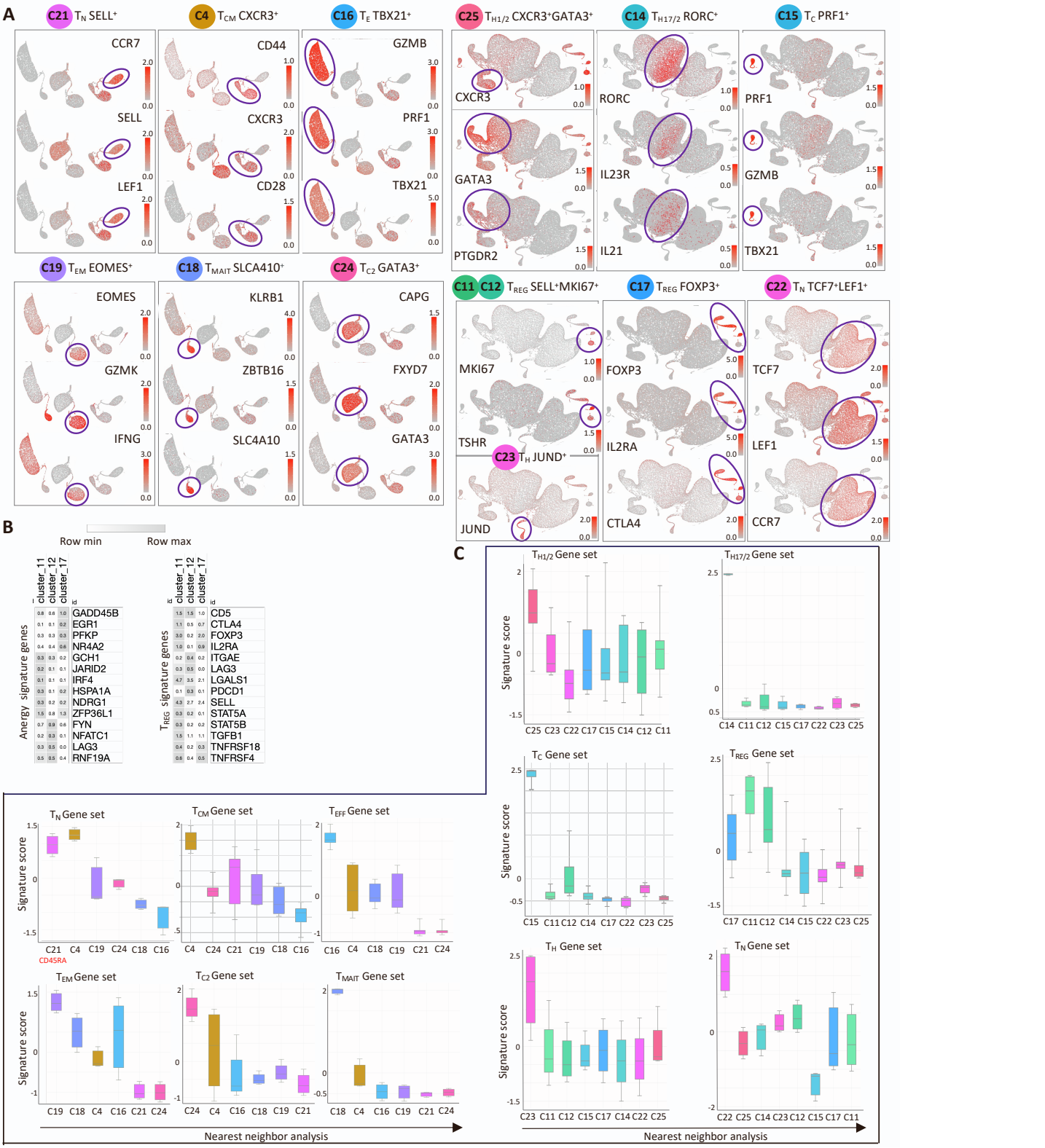

Supplemental figure 2. Gene markers of T cell subsets, related to figure 2. (A) KNetL plots projecting the RNA expression of marker genes indicated in red. Each red dot represents a cell. (B) Heatmap representation of RNA expression of anergy and T_{REG} marker genes sets. (C) Bar graphs indicting the marker gene sets score for each subset cluster, further resolved in the basis of nearest between the marker gene sets.

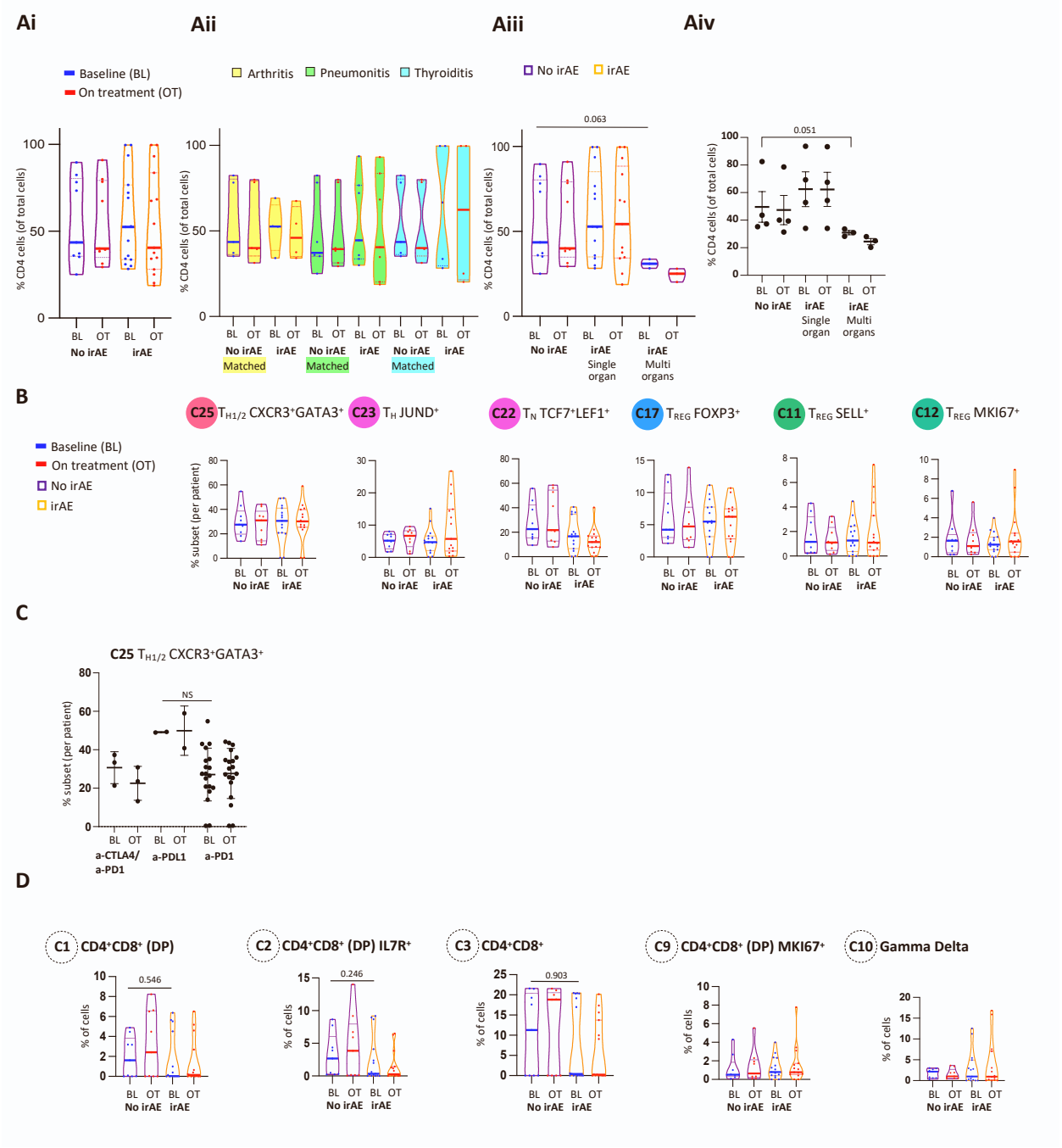

Supplemental figure 3. Characterization of CD4 T cells, related to figure 3. Percentages distribution of subset of CD4 T cells between no irAE and the different irAE groups of patients at baseline and on treatment (A). Percentages of CD4 specific clusters among patients with and without irAEs and baseline and on treatment with ICIs (B). Percentages of cells of cluster 25 based on the specific type of ICIs used (C). Double positive and gamma delta T cells (D).

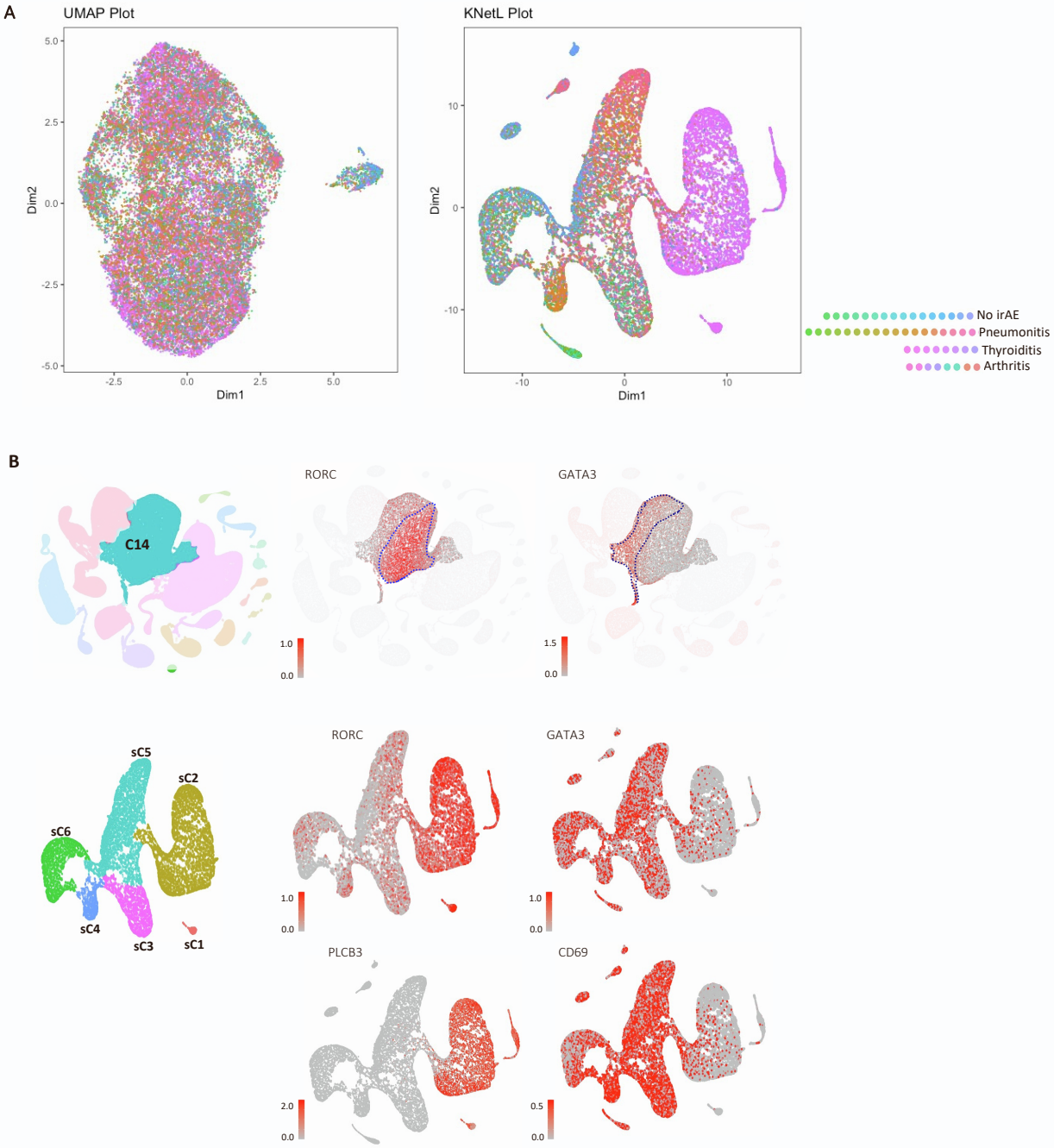

Supplemental figure 4. Characterization of the T cells in cluster 14, related to figure 4. (A) UMAP and KNetL projections of cells from sub-clustering of meta-cluster 14. (B) KNetL projection of marker gene RORC, GATA3, PLCB3, and CD69.

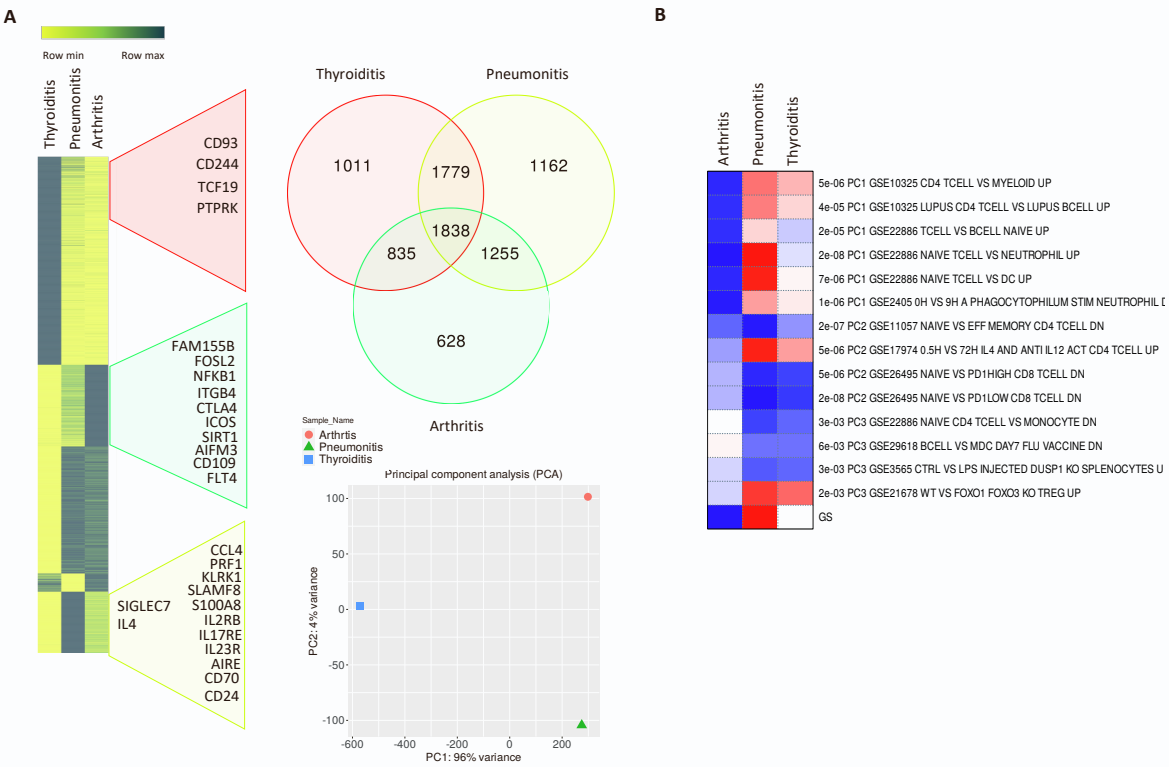

Supplemental figure 5. Organ specific toxicities and association with gene expression, related to figure 4. Heat map, Venn diagram, and PCA plot of the different genes that characterize patient with arthritis, thyroiditis and pneumonitis irAEs (A). Comparison of organ specific irAEs genes and published GSE studies (B).

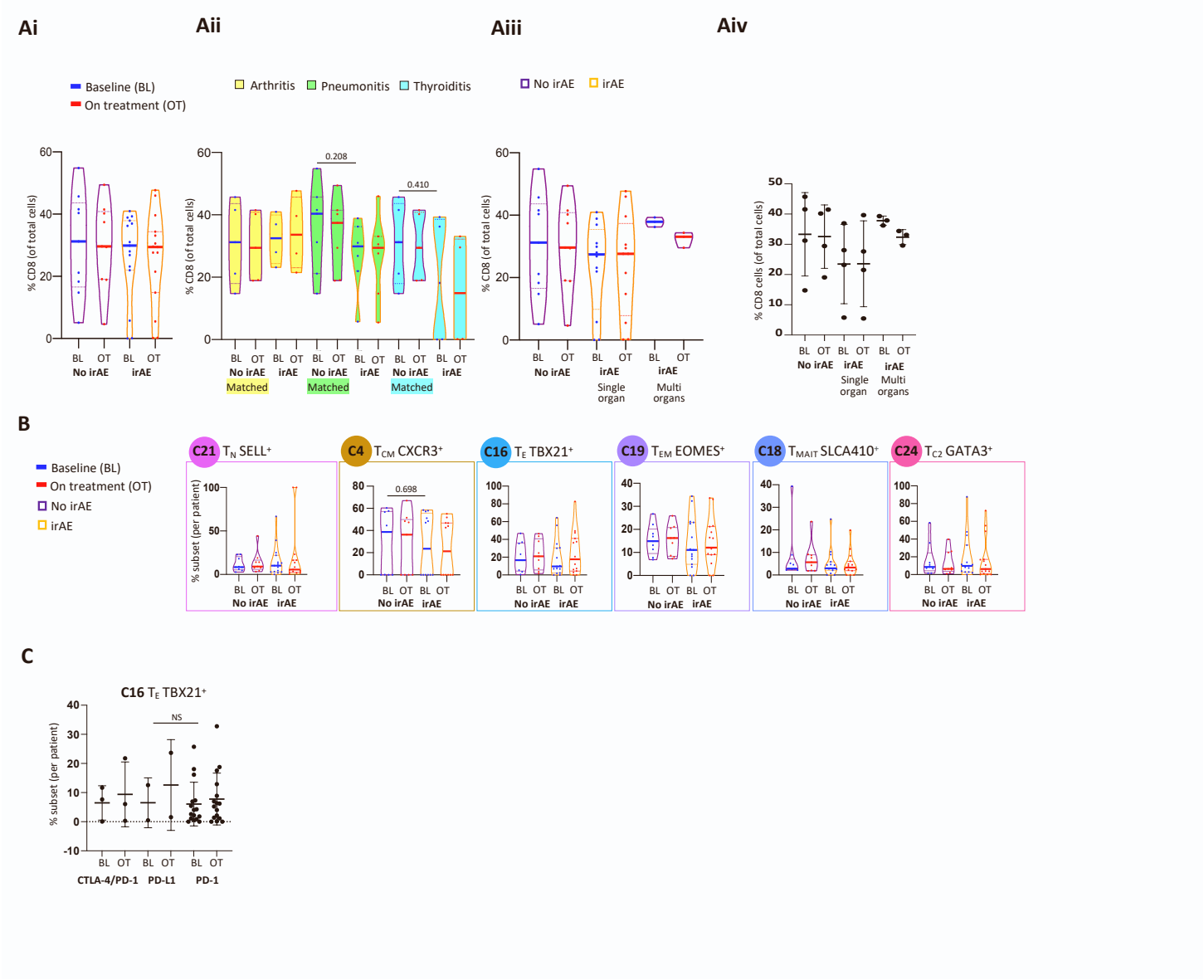

Supplemental figure 6. Characterization of CD8 T cells, related to figure 5. Percentages of CD8 cell clusters among patients with different types of irAEs (A). Percentages of specific clusters of cells of patients with and without irAEs. Percentages of subset of patients treated with different types of ICIs (C).

A

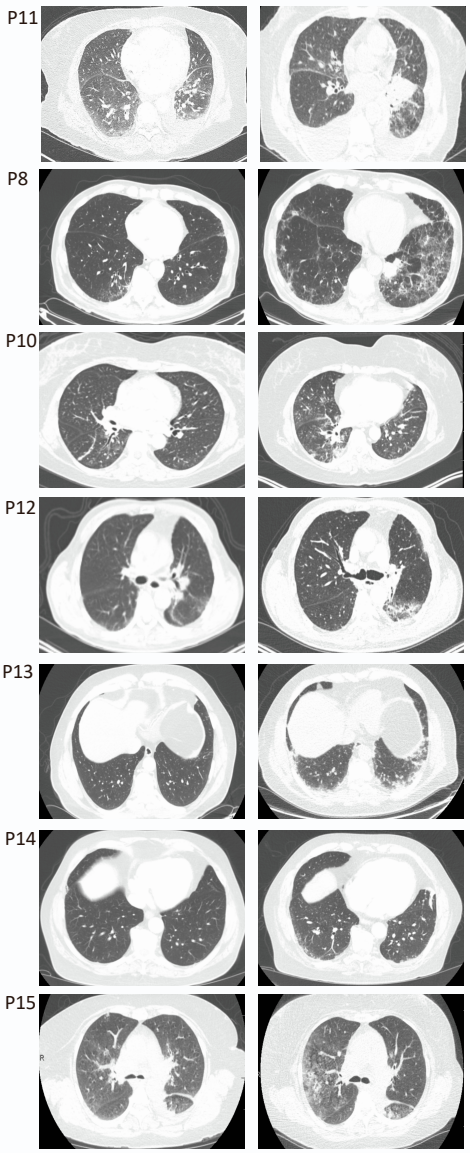

B

Patient No.	Pneumonitis Pattern	Tumor type	irAE grade	Size Dominant nodule (mm)	Location of nodule
P8	CHP	NSCLC	2	26	LUL
P10	CHP	NSCLC	3	77	RLL
P11	CHP	NSCLC	2	37	RLL
P12	OP	NSCLC	2	18	LLL
P13	OP	Prostate	3	0	NA
P14	OP	Prostate	3	0	NA
P15	OP	NSCLC	3	67	LLL

Supplemental figure 7. CT scans of pneumonitis patients at baseline and on treatment, related to figure 6. CT scan images (A). Clinical characterization of irAE patients that developed pneumonitis (B).